POLITECNICO DI TORINO
Repository ISTITUZIONALE

Multiscale models for movement in oriented environments and their application to hilltopping in butterflies

(Article begins on next page)

17 May 2024

Multiscale models for movement in oriented environments and their application to hilltopping in butterflies

Kevin J Painter

Preprint version: July 23, 2013

Abstract Hilltopping butterflies direct their movement in response to topography, facilitating mating encounters via accumulation at summits. In this paper, we take hilltopping as a case-study to explore the impact of complex orienteering cues on population dynamics. The modelling employs a standard multiscale framework, in which an individual's movement path is described as a stochastic 'velocity-jump' process and scaling applied to generate a macroscopic model capable of simulating large populations in landscapes. In this manner, the terms and parameters of the macroscopic model directly relate to statistical inputs of the individual-level model (mean speeds, turning rates and turning distributions). Applied to hilltopping in butterflies, we demonstrate how hilltopping acts to aggregate populations at summits, optimising mating for low density species. However, for abundant populations hilltopping is not only less effective, but possibly disadvantageous, with hilltopping males recording a lower mating-rate than their non-hilltopping competitors.

Keywords: oriented movement; topographical cues; multiscale models; butterfly populations; mate location.

1 Introduction

Natural environments are replete with cues that provide useful orienteering information: topography and landmarks, chemical, magnetic and electric fields, and so on. The question of how an evolving, heterogeneous and anisotropic environment is filtered and exploited by an individual is quite clearly a complex and difficult one, yet the answer is essential for understanding the spatial organisation of a population and, in turn, population dynamics. 'Hilltopping' is a phenomenon associated with a number of butterfly species (and other flying insects), in which individuals orient in response to topography and accumulate at summits (Shields 1967; Scott 1968; Alcock 1987). The short lifespan of many butterflies places a significant pressure to mate, and their susceptibility to a wide variety of factors, including climate, habitat, parasitism and predation, can generate significant variations between one year and another: consequently, their dynamics provide an important model for evaluating the robustness of populations in general, e.g. see Ehrlich and Hanski (2004). Efficient mate-locating strategies, particularly for low density species, are a must and hilltopping, in which peaks act as foci for newly emerging females, offers one such mechanism. Consequently,

Department of Mathematics and Maxwell Institute for Mathematical Sciences, Heriot-Watt University, Edinburgh, EH14 4AS, UK. Tel: +44 131 4518234, Fax: +44 131 4513249
E-mail: K.Painter@hw.ac.uk

hilltopping has been the focus of a number of field studies (Shields 1967; Scott 1968; Ehrlich and Wheye 1986; Alcock 1987; Baughman et al. 1988; Wickman 1988; Turchin et al. 1991; Pe'er et al. 2004), revealing its important role in determining population structure.

Insight into the orienteering cues used by organisms is typically obtained from tracking, whether through traditional field tracking (e.g. Turchin et al. 1991) or more recent technologies (e.g. harmonic radar, Cant et al. 2005, or global positioning systems (GPS), Tomkiewicz et al. 2010). In the context of butterfly flight, tracking an individual and recording its landing (or turning) location generates an approximated movement path that can be quantified by various statistics: mean travel speeds; persistence of direction; frequency of turning and turning distributions. Correlation with the local terrain can indicate a tendency to utilise topography for orienteering (Turchin et al. 1991; Pe'er 2003; Pe'er et al. 2004).

Field studies are always subject to an element of uncertainty, even when stringently conducted. Modelling is unencumbered by such noise: real-world complexity can be replaced with a precisely defined and controlled 'environment', although the results following such reductionism must obviously be interpreted with care. Nevertheless, modelling can be used to test specific hypotheses and explore particular questions: for example, to what extent does hilltopping increase the mating success of a butterfly population, or does following this strategy always pay off?

Formulating a spatial model to answer such questions is, naturally, dependent on the relevant scale of interest and the available data. The questions above are posed at the population-level, yet movement data is obtained through tracking individuals. The latter naturally implies an individual-based (or agent-based) model, in which each individual is described by a separate object that moves through (and interacts with) its environment according to a set of rules motivated by hypothesised behaviour. Yet the reliance of such approaches on raw computational power can be problematic for large numbers in extended environments.

Modelling at a population, or macroscopic, level involves painting with a broader brush, for example through equations for the evolution of population densities, structured by position and time: the finer details of an individual's movement path are condensed into net dispersal terms. In meta-population models, the structure of a global population on a landscape is described by a spatially-discrete network of local populations, linked through global dispersal (e.g. see Hanski 1999). In spatially-continuous models (see Cantrell and Cosner 2004), a population is typically modelled via a continuous density distribution. For example, letting $u(t, \mathbf{x})$ denote the population density of the modelled species at position $\mathbf{x}$ and time t, one approach is to postulate a partial differential equation for the rate of change of $u(t, \mathbf{x})$ of the form

$$u_t = -\nabla \cdot \mathbf{J}(t, \mathbf{x}) + f(u, t, \mathbf{x}), \tag{1}$$

where right-hand side terms denote movement and kinetics, respectively. Various movement classes can be modelled through the choice for the net population flux, $\mathbf{J}(t, \mathbf{x})$. For example, if movement is considered to be essentially random, a classic assumption is a Fickian-style diffusive flux $\mathbf{J} = -d\nabla u$, where d defines the diffusion coefficient (e.g. Cantrell and Cosner 2004).

Macroscopic spatial models have tremendous power: with a root planted in classical applied mathematics, standard analytical techniques can provide a nuanced understanding of how spatial structure evolves over generations, with less reliance placed on brute-force computation. However, their connection to the properties of an individual's movement is blurred: in the context of (1), what are the *appropriate* flux terms to describe a particular form of movement and what are the relationships between macroscopic parameters, such as the diffusion coefficient, and the statistical quantities obtained from individual-level data?

Reconciling population-level models with individual-level data can be achieved using a multiscale approach: for example, an individual-based model is formulated and scaling arguments employed to bridge the gap to the corresponding macroscopic model. Moreover, simultaneous computations of individual-based and continuous models provide distinct perspectives on the properties
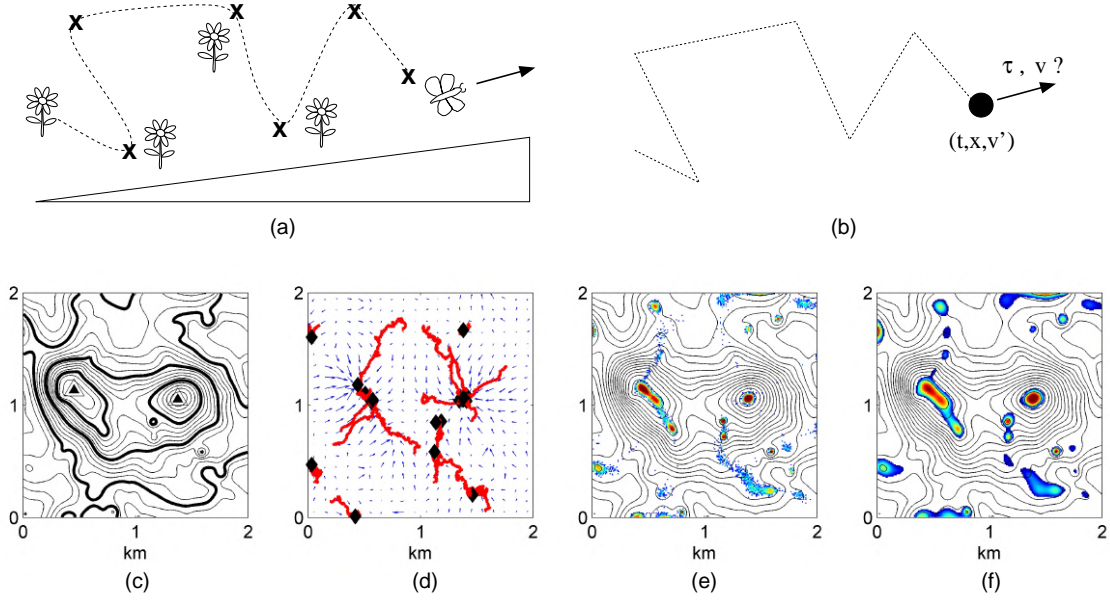
Fig. 1 Illustration of the modelling framework: (a) representative flightpath for the localised movement of a hilltopping butterfly; (b) discretisation as a velocity-jump random walk (see Section 2.1); (c) contour representation of a topographically complex landscape, with triangles marking major summits (see Figure 3); (d) representative trajectories of virtual hilltopping butterflies (two days, final locations illustrated by diamonds), involving oriented movement to local topography (gradient of the landscape in (c) illustrated by arrows); (e) two-day distribution of an initially dispersed population reveals its structuring into hilltop aggregates; (f) the macroscopic model accurately recapitulates this distribution. See text for details.

of a system. Adopting such methods requires assumptions and approximations, and a careful evaluation of their validity forms an essential component of the modelling process. Nevertheless, a direct and transparent pathway is laid out between the statistical data informing the individual model and the terms and parameter inputs of the macroscopic model.

1.1 Outline

In this paper we expound a multiscale framework for modelling animal movement within complex environments via an application to butterfly hilltopping. The modelling is founded on a stochastic 'velocity-jump' random walk model (Othmer et al. 1988) for individual movement paths. In the formulation here, laid out in detail in Hillen and Painter (2013), orienteering cues – such as topography for hilltopping butterflies – impart directional information via an appropriate contribution to the probability distribution for a new velocity/direction. We state the scaling that leads to a macroscopic model: an anisotropic drift-diffusion equation parametrised by the statistical properties of the underlying individual model. Tailored to butterfly hilltopping, we demonstrate the accumulation of a virtual population at hilltops and, exploiting its advantages, extend the macroscopic model to account for mating dynamics. Our modelling substantiates the hypothesis that hilltopping strategies are particularly effective for low density species. For abundant species, however, pursuing a hilltopping strategy is shown to be unfavourable for individual males, with non-hilltopping competitors demonstrating greater mating success.

The methodology is illustrated in Figure 1. A typical butterfly movement path is illustrated in (a): if hilltopping occurs, movement is generally in an uphill direction. Portrayed as a velocity-

jump random walk, this path is discretised into running and turning, where at each turn a butterfly 'selects' a new velocity (v) and flight time (τ) according to appropriate probability distributions. The impact of orienteering cues in the environment, such as the topologically-complex terrain (c) for hilltopping butterflies, can be incorporated via appropriate inputs into these distributions: for hilltopping, we propose that the velocity chosen by an individual is biased according to the direction and steepness of the local gradient, illustrated for the landscape in (c) by the direction and length of arrows in (d). Movement paths of virtual butterflies, computed through direct stochastic simulation of the velocity-jump model, generally follow this information. For a large and initially dispersed population, accumulation at summits is observed, (e). At this landscape scale, macroscopic equations for the population density, derived by scaling, recapitulate the distribution predicted by the individual model, (f).

2 Multiscale modelling of movement paths

To motivate the modelling that follows, we briefly describe findings from a field study (Pe'er 2003; Pe'er et al. 2004) of the hilltopping butterfly *Melitaea trivia*. This species, distributed widely in Southern Europe and the Middle East, has been the subject of an intensive tracking study during spring 2000 in southern Israel ($31°25'N, 34°50'E$). Movement paths of released individuals were recorded via the sequential flagging of landing/turning locations, with analysis indicating that male and virgin female butterflies generally (but not ubiquitously) select an up-slope direction following a landing, with mated females showing no such tendency: consistent with the general hypothesis that hilltopping is primarily exploited to facilitate mating and 'switched-off' when not required. Furthermore, the timing or frequency of turns showed no significant dependence on the local slope, with a distribution statistically indistinguishable from a Poisson process.

To describe such movements, and their impact on population structure, we formulate a series of discrete and continuous models, operating over distinct spatial scales: (Ia) an **individual-based** (or agent-based) stochastic model; (Ib) its continuous and deterministic equivalent, a **mesoscopic velocity-jump** model; and (II) a continuous **macroscopic model**, operating at the scale of movement of a population over a landscape. Noting the substantial existing literature on the use of random walk models to describe animal or cell movement (e.g. see Skellam 1951; Patlak 1953; Kareiva and Shigesada 1983; Othmer et al. 1988; Turchin 1998; Okubo and Levin 2001; Codling et al. 2008; Othmer and Xue 2013 and references therein), here we employ the velocity-jump model (Othmer et al. 1988): movement is assumed to alternate between *running* (movement with constant velocity) and *turning* (selecting a new velocity). This natural model for movement is clearly compatible with standard descriptions for recording animal paths, and hence can be parametrised by field data: butterfly movement consists of a sequence of discrete movements and the path laid out by recording the times and locations of landing sites closely fits that of the velocity-jump type model, e.g. see Turchin et al. (1991).

Beginning with the underlying velocity-jump process, we refine to a simpler and more convenient form that remains relevant for the current application: specifically, it incorporates the impact of a complex (topographic) environment on movement paths, yet admits a straightforward route to a fully macroscopic model. We note that the formulation itself is not novel: we follow that laid out in Hillen and Painter (2013) and a number of details will be omitted for succinctness. Further details of velocity-jump (and other random-walk) models of biological movement and their applications can be found in the general reviews of Codling et al. (2008); Othmer and Xue (2013).

2.1 (I) Individual and velocity-jump models

We let t denote time, $\mathbf{x} \in \mathbb{R}^d$ the spatial coordinate ($\mathbf{x} = (x, y)$ for $d = 2$) and $\mathbf{v} \in \mathbb{R}^d$ the velocity. While we currently remain in general form, we note that for butterflies (which typically remain a few metres within the ground) $d = 2$ would be appropriate. We assume individuals move within a range of speeds $[s_1, s_2]$ (where $0 \leq s_1 \leq s_2 < \infty$) and that turns/velocity changes occur as a Poisson process, where $\tau(t, \mathbf{x})$ denotes the *mean runtime* between velocity changes (and $\lambda = 1/\tau$ is the *turning rate*). At each turn, an individual selects a new velocity $\mathbf{v}$ according to the probability distribution $q(t, \mathbf{x}, \mathbf{v}, \mathbf{v}')$, where $\mathbf{v}'$ is the previous velocity. Clearly,

$$\int_V q(t, \mathbf{x}, \mathbf{v}, \mathbf{v}')d\mathbf{v} = 1 \,.$$

This individual-based model can be formulated as a mesoscopic velocity-jump model (Othmer et al. 1988): formally this describes a probability distribution for the position of an individual, but it can be interpreted as an evolution equation for population densities. Specifically, letting $p(t, \mathbf{x}, \mathbf{v})$ denote the population density of organisms at time $t \geq 0$, location $\mathbf{x}$ and moving with velocity $\mathbf{v}$, evolution of $p(t, \mathbf{x}, \mathbf{v})$ is given by

$$p_t(t, \mathbf{x}, \mathbf{v}) + \overbrace{\nabla \cdot \mathbf{v}p(t, \mathbf{x}, \mathbf{v})}^{\text{running}} = \overbrace{\frac{1}{\tau(t, \mathbf{x})} \left(\int_V q(t, \mathbf{x}, \mathbf{v}, \mathbf{v}')p(t, \mathbf{x}, \mathbf{v}')d\mathbf{v}' - p(t, \mathbf{x}, \mathbf{v}) \right)}^{\text{turning}}, \qquad (2)$$

where the index t denotes the partial time derivative. On the right hand side, turning is split into an integral term for switching into velocity $\mathbf{v}$, and a term for switching out of velocity $\mathbf{v}$. Formal derivations are considerably less straightforward if interactions (direct or indirect) between individuals must be taken into account: we remark on this further in the discussion.

2.2 Simplified individual and velocity-jump models

In general, both turning rates and reorientation distributions vary according to internal (e.g. previous velocity) and environmental (e.g. due to orienteering cues) factors: a specific application therefore demands close scrutiny of the available data to ensure suitable functional forms are selected. In the formulation considered in Hillen and Painter (2013), it was assumed that (i) the mean runtime τ (or turning rate) is independent of other factors, i.e $\tau = $ constant; and (ii) the choice of new velocity does not depend on the previous velocity $\mathbf{v}'$, i.e. $q(t, \mathbf{x}, \mathbf{v}, \mathbf{v}') = q(t, \mathbf{x}, \mathbf{v})$. In the later application to butterfly hilltopping, these simplifications appear acceptable given the flight path characteristics and data available in Pe'er et al. (2004): butterflies land between turnings, and any contribution from the pre-landing velocity can therefore be assumed to be relatively small; data analysis revealed that local topography impacts on the choice of a butterfly's new orientation (i.e. q) but there was no demonstrated link to the frequency of landings (i.e. λ or τ).

As a final simplification we assume that (iii) individuals travel with a fixed mean speed s (i.e. $s_1 = s_2 = s$), and hence $\mathbf{v} = s\mathbf{n}$ for direction $\mathbf{n} \in \mathbb{S}^{d-1}$. For butterflies this could be an actual flight speed, if butterflies alight only briefly at turns and the time scale of interest is short, or a mean path speed averaged over a much longer time interval. The latter would absorb the (potentially considerable) time taken for other activities, such as resting, sheltering and feeding, and the paths generated would not represent real flight paths as such, rather the effective path that traces out the butterfly's passage over the landscape. A more sophisticated approach would be to explicitly split individuals into moving and resting subpopulations (e.g. see Othmer et al. 1988; Hillen 2003), however we do not consider this complication at present.

We note that while the various assumptions above can be relaxed, the subsequent derivation of a macroscopic model can not be guaranteed and would require a separate treatment. In terms of the mesoscopic velocity-jump model, these assumptions allow us to reduce (2) to the simpler form (Hillen and Painter 2013):

$$p_t(t, \mathbf{x}, \mathbf{v}) + \nabla \cdot \mathbf{v}p(t, \mathbf{x}, \mathbf{v}) = \frac{u(t, \mathbf{x})q(t, \mathbf{x}, \mathbf{v}) - p(t, \mathbf{x}, \mathbf{v})}{\tau} \,, \tag{3}$$

where τ is now a constant. We note that $u(t, \mathbf{x})$ defines the observable or *macroscopic population density*

$$u(t, \mathbf{x}) = \int_V p(t, \mathbf{x}, \mathbf{v})d\mathbf{v} \,.$$

Furthermore, since individuals travel with a fixed mean speed s, the *turning distribution q* (for choosing a new velocity $\mathbf{v} \in V(= s\mathbb{S}^{d-1})$) can be reinterpreted as a *directional distribution*, $\tilde{q}(t, \mathbf{x}, \mathbf{n})$, on the unit sphere $\mathbb{S}^{d-1}$: $\tilde{q}(t, \mathbf{x}, \mathbf{n})$ defines the probability of choosing a new direction $\mathbf{n} \in \mathbb{S}^{d-1}$. Specifically,

$$q(t, \mathbf{x}, \mathbf{v}) := \frac{\tilde{q}(t, \mathbf{x}, \mathbf{n})}{s^{d-1}} \text{ where } \int_{\mathbb{S}^{d-1}} \tilde{q}(t, \mathbf{x}, \mathbf{n})d\mathbf{n} = 1 \,. \tag{4}$$

2.3 (II) The macroscopic description

In certain applications it may be either appropriate or more convenient to work directly with the previous models – for example, if population numbers are low or if the spatial/temporal scales of interest occur at the level of an individual's movement – yet this comes at a cost of greater computational expanse and reduced analytical tractability.

In many cases the spatial and temporal scales of interest are distinct and a macroscopic model can be obtained through scaling: in hilltopping, butterflies typically fly a few metres and turn/land once every minute or so, yet overall population dynamics evolve on a landscape of the order of kilometres and flight seasons of the order of weeks. From a population biology perspective, we are less concerned of the success of one individual, rather the overall success of the population and it is desirous to obtain an appropriate model for the macroscopic population density, $u(t, \mathbf{x})$. Scaling provides a route from the functions and parameters of the individual model (e.g. speeds, turning rates and distributions) to the terms and inputs of the macroscopic model for $u(t, \mathbf{x})$. Inevitably this entails approximations, loss of information and a coarser model results: the validity of any approximations should be considered with care.

We do not consider the intricacies of scaling here (referring to Hillen and Painter (2013) and references therein for details), simply noting that a variety of methodologies can be adopted. Here we employ a *moment closure approach* and adopt a *fast-flux relaxation*: this method originates in a physical context, and its translation to a biological setting must be interpreted accordingly. Briefly, a series of equations is formulated for variables including the population density (i.e. u, or mass in the physical context) and average population flux (or momentum). Each new equation requires an additional variable (or moment), and assumptions must be made for closure. In the fast-flux relaxation the system is taken to be close to equilibrium, and the population flux is assumed to rapidly equilibrate: effectively, the local population flux is taken to correlate with the local orienteering information obtained from the environment. The validity of this assumption clearly relates to scale: for example, failing at the mesoscopic-scale of the velocity-jump model, where an individual transits over changes in orienteering information during the run phase, only re-evaluating the environment at a turn. We later illustrate the validity of the scaling via numerical comparisons (see Figures 2 and 5) of the individual-based, mesoscopic and macroscopic models.

Applied to (3), moment closure generates a macroscopic model in the form of the drift-anisotropic diffusion model:

$$u(t,\mathbf{x})_t + \nabla \cdot \mathbf{a}(t,\mathbf{x})u(t,\mathbf{x}) = \nabla\nabla\left(\bar{D}(t,\mathbf{x})u(t,\mathbf{x})\right). \tag{5}$$

In the above $\bar{D}(t,\mathbf{x})$ defines a (symmetric) $d \times d$–diffusion tensor matrix, $\mathbf{a}(t,\mathbf{x})$ is the d–dimensional drift (or advective) velocity. For the right hand side, we use the notation

$$\nabla\nabla(\bar{D}u) = \sum_{i,j=1}^{d} \frac{\partial}{\partial x_i}\frac{\partial}{\partial x_j}(\bar{D}^{ij}u).$$

Notably, each of the macroscopic quantities $\mathbf{a}$ and $\bar{D}$ are determined according to the statistical properties of the inputs for the velocity-jump process: mean speeds, run times and turning distributions. In particular, we note that the drift $\mathbf{a}$ is the *expectation* (i.e. the weighted average velocity) of q, while $\bar{D}$ is proportional to the *variance-covariance matrix* (the higher-dimensional analogue of variance) of q. Specifically,

$$\mathbf{a}(t,\mathbf{x}) = \int_V \mathbf{v}q(t,\mathbf{x},\mathbf{v})d\mathbf{v} = s\int_{\mathbb{S}^{d-1}} \mathbf{n}\tilde{q}(t,\mathbf{x},\mathbf{n})d\mathbf{n}, \tag{6}$$

$$\bar{D}(t,\mathbf{x}) = \tau\int_V (\mathbf{v}-\mathbf{a}(t,\mathbf{x}))(\mathbf{v}-\mathbf{a}(t,\mathbf{x}))^T q(t,\mathbf{x},\mathbf{v})d\mathbf{v},$$

$$= \tau s^2 \int_{\mathbb{S}^{d-1}} (\mathbf{n}-\mathbf{a}(t,\mathbf{x})/s)(\mathbf{n}-\mathbf{a}(t,\mathbf{x})/s)^T \tilde{q}(t,\mathbf{x},\mathbf{n})d\mathbf{n}. \tag{7}$$

Note that the product $\mathbf{v}\mathbf{v}^T$ denotes the dyadic product of two vectors and therefore generates a (symmetric) matrix.

As a point of note, the diffusion term in (5) is distinct from that of 'classic' anisotropic diffusion:

$$u_t = \nabla(\bar{D}\nabla u).$$

The 'fully-anisotropic' form in (5) arises naturally from the underlying transport equation and has significant ramifications on population patterning: it holds additional advective-type terms that aggregates populations at interfaces of varying anisotropy (see Hillen and Painter 2013; Hillen et al. 2013; Painter and Hillen 2013 for examples in a biological context).

2.4 Incorporating orienteering cues

In the simplified velocity-jump process here, flexibility lies in the choice of q (or $\tilde{q}$) and we assume orienteering cues, potentially varying with position and time, are encoded into this distribution: for a hilltopping butterfly, an appropriate response to a measure of the topography (e.g. gradient) would be accounted for in q. Orienteering cues that are altered by individuals – such as released pheromones – would require separate evolution equations for their dynamics.

Linking the turning distribution to the macroscopic drift vector and diffusion tensor is illustrated through some apposite examples. In line with the later application, we restrict to a two-dimensional region: $d = 2$, $\mathbf{x} = (x,y)$ and $\mathbf{v} = s\mathbf{n} = s(\cos\theta, \sin\theta)$, where angle $\theta \in (-\pi, \pi]$. Hence we specify a directional distribution $\tilde{q}(t,x,y,\theta)$ on the unit circle, related to the turning distribution via $q(t,x,y,\mathbf{v}) := \frac{\tilde{q}(t,x,y,\theta)}{s}$.

For a single preferred direction of turning – such as uphill for hilltopping butterflies – a natural description is the von Mises distribution (e.g. Mardia and Jupp 2000), a form of normal distribution wrapped onto the unit circle:

$$\tilde{q}(\theta \mid k, \phi) = \frac{1}{2\pi I_0(k)} e^{k\cos(\theta-\phi)} \, . \tag{8}$$

The above generates a predominance of turns into the direction corresponding to the dominant angle, ϕ, concentrated according to k; $I_j(k)$ denotes the modified Bessel function of first kind of order j. We refer to Moorcroft and Lewis (2006); McKenzie et al. (2012); Hillen and Painter (2013); Painter and Hillen (2013) for applications in biological movement ranging between cells and organisms. Generally, $\phi(t, x, y)$ and $k(t, x, y)$ are functions of space and time to reflect variation in the direction and strength of the orienteering cue: these dependencies are omitted from the notation for clearer presentation.

Expectations and variance-covariance matrices of (8) have been previously calculated (e.g. see Hillen and Painter 2013) and we can therefore state explicit forms for the drift-velocity and diffusion tensor in (5) according to the dominant angle and concentration parameter:

$$\mathbf{a}(k, \phi) = s\frac{I_1(k)}{I_0(k)}(\cos\phi, \sin\phi) \, , \tag{9}$$

$$\bar{D}(k, \phi) = \frac{\tau s^2}{2} \left(1 - \frac{I_2(k)}{I_0(k)}\right) \begin{pmatrix} 1 & 0 \\ 0 & 1 \end{pmatrix}$$
$$+ \tau s^2 \left(\frac{I_2(k)}{I_0(k)} - \frac{I_1(k)^2}{I_0(k)^2}\right) \begin{pmatrix} \cos^2\phi & \cos\phi\sin\phi \\ \cos\phi\sin\phi & \sin^2\phi \end{pmatrix} \, . \tag{10}$$

The drift is as expected: in the direction corresponding to the dominant angle. The anisotropic diffusion tensor has been decomposed into isotropic and anisotropic terms, where the alignment of the latter also depends on the dominant angle. We first note that as $k \to 0$, the directional distribution $\tilde{q}$ becomes uniform and all directions are chosen equally. In this limit, $\frac{I_1(k)}{I_0(k)}, \frac{I_2(k)}{I_0(k)} \to 0$, the drift term disappears and diffusion, as to be expected, becomes isotropic. As $k \to \infty$ an individual becomes increasingly restricted into choosing angle ϕ: $\frac{I_1(k)}{I_0(k)}, \frac{I_2(k)}{I_0(k)} \to 1$, diffusion terms disappear. This limiting scenario corresponds to a pure-drift equation in which the local population density is advected in the direction indicated by $\phi(x, y, t)$, for example the direction of the local gradient.

Although the above treatment is specific to the two-dimensional case, other applications may demand a full three-dimensional treatment. The natural extension of (8) to higher dimensions is the Fisher-von Mises distribution (Mardia and Jupp 2000): its expectation and variance co-variance matrix and, hence, corresponding drift and anisotropic diffusion tensors for input into the macroscopic model (5) can be found in Painter and Hillen (2013). Note that the forms (9)–(10) have also been determined in other studies for biological movement, albeit under a different starting random walk model (e.g. Codling et al. 2010).

We also note that many environments feature multiple orienteering cues: for example, a butterfly's movement can also be influenced by pheromones, vegetation, wind and other factors (Dover and Settele 2009). One approach to model environments with multiple cues would be to apply linear combinations of (8), parametrised distinctly to represent the different orienteering fields.

2.5 Numerical case study

We conclude this section with a brief case study: motivated by hilltopping and other types of gradient-following, but idealised such that important elements of the modelling process can be

exhibited. In line with later applications we will restrict to time-independent orienteering cues, and remove the $t-$dependence where applicable for notational simplicity. We further restrict to a rectangular landscape $A = [0, L_x] \times [0, L_y] \in \mathbb{R}^2$ containing a population of individuals. To conserve the population, we assume zero net-loss at the boundaries: for the individual and mesoscopic models, an individual moving out of the region with velocity $\mathbf{v}$ is instantaneously replaced (or reflected) by another individual moving into the region at the same location and with velocity $-\mathbf{v}$; in the corresponding macroscopic model this translates to zero-flux boundary conditions.

We consider a single orienteering cue in A that provides taxis-type attraction via gradient following: in the context of butterflies, this could represent a hilltop or pheromone source. We denote the orienteering cue $E(x, y)$ and assume individuals orient according to the local gradient ∇E: the angle $\phi(x, y)$ in (8) is taken in the direction of ∇E and we assume steeper gradients generate a higher tendency to take this direction,

$$k(x, y) = \kappa \left| \nabla E(x, y) \right| . \tag{11}$$

The sensitivity parameter κ indicates the capacity to detect and follow the gradient. We note that it is straightforward to consider more sophisticated sensing mechanisms: for example, the individual may sample E over some non-local region determined by its sensory range.

To generate a quasi-one-dimensional framework, we assume a population is initially distributed uniformly with x and E only varies with y: specifically, $E(y) = E_0 e^{-a(y-y_0)^2}$ (for $a, y_0, E_0 > 0$). Hence, $\phi = \pm\frac{\pi}{2}$ for $y \lessgtr y_0$ and dominant turning will be in the direction of the 'ridge', $y = y_0$. With (11), drift and diffusion tensors are calculated from (9–10) as follows:

$$\mathbf{a}(x, y) = (0, sa(y)), \quad \bar{D}(x, y) = \begin{pmatrix} \tau s^2 d_1(y) & 0 \\ 0 & \tau s^2 d_2(y) \end{pmatrix}, \tag{12}$$

where coefficients $a(y), d_1(y)$ and $d_2(y)$ depend on y via k. Figure 2 (a) illustrates the translation between E and these coefficients, via $\tilde{q}$. The turning distribution illustrates a predominance of turns towards y_0, concentrated according to the local steepness of E. The drift is clearly towards $y = y_0$ while the diffusion tensor coefficients vary across the field; their distinct sizes in regions of steep gradient imply anisotropic diffusion.

We simulate the predicted movement of a population: 100 individuals are released, initially distributed uniformly across A. Figure 2 (b) shows typical simulations of the stochastic individual-based model: the tendency of individuals to orient according to the gradient of E is clear, culminating in accumulation along the ridge $y = y_0$. Exploiting the quasi-one-dimensional framework, we investigate model convergence: obtaining (5) demands that the scale of interest is 'appropriately macroscopic', and we should only expect correspondence within suitable parameter regimes. Averaging over x and computing the evolving density distributions as functions of y, we compare the stochastic simulations of the individual-based model with numerical solutions of the mesoscopic velocity-jump model (3), and the macroscopic model (5). In each case the population is normalised to yield a dimensionless average density ($=1$), while distributions predicted from the stochastic model are averaged over multiple (1000) simulations. Note that τ, κ and the parameters defining E are fixed, leaving s as a control parameter.

The results plotted in Figure 2 (c) clearly indicate model convergence, although only in certain parameter regimes: smaller s yields a quasi-identical match, yet larger values lead to significant discrepancy between the macroscopic and individual/mesoscopic models. Intuitively, when $s = 1.0$ (and $\tau = 1.0$) the mean distance travelled by an individual between turns is $\tau s = 1$: the observation frame is the order of an individual movement path and the macroscopic model (5) has little import. For smaller s, e.g. $s \lesssim 0.01$, the average path lengths forms a fraction of the length scales of A and the macroscopic viewpoint is valid.
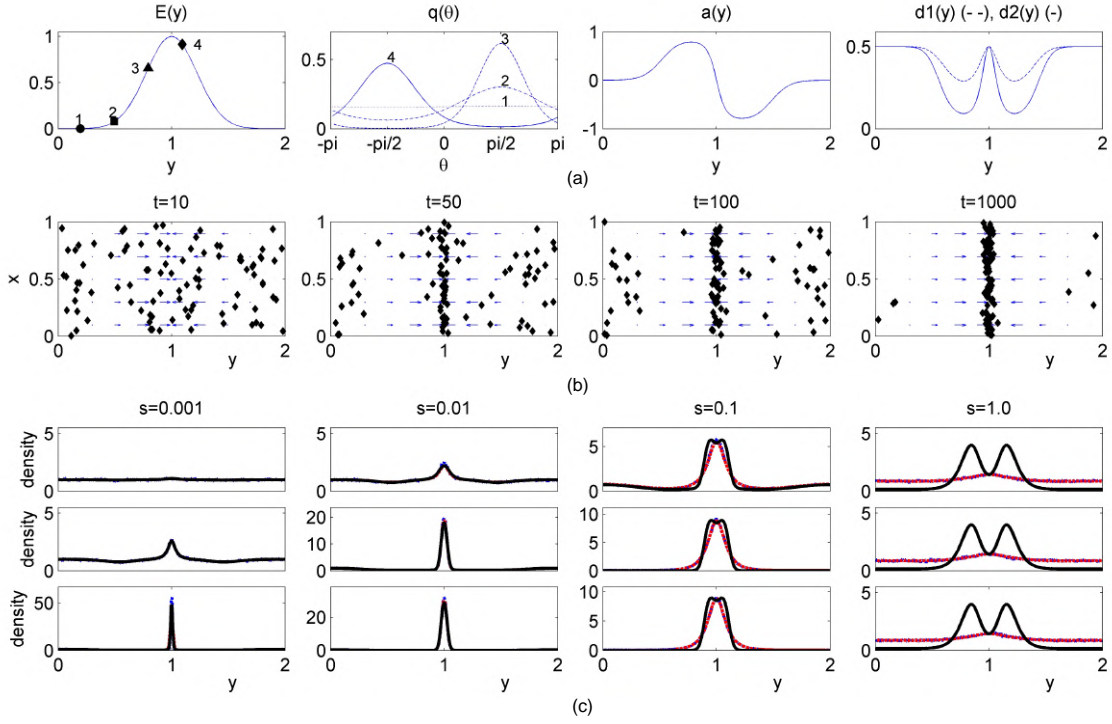
Fig. 2 (a) Translation from orienteering cue to inputs for the macroscopic model: (left) individuals are assumed to move up gradients of the cue $E(y)$; (centre-left) the turning distribution is shown for the points along the y-axis indicated, we note that the dominating direction and concentration of turning vary along y; (centre-right) drift-vector and (right) diffusion-tensor coefficients generated from E(y), revealing drift towards $y = y_0 (= 1)$ and anisotropic diffusion. (b) Stochastic simulations of the individual-based model for a population (of size 100) responding to the gradient of $E(y)$: the direction and steepness of the latter is reflected in the underlying arrows. We observe accumulation of individuals along the ridge $y = y_0$. Individuals were initially positioned uniformly across A, other parameters listed below. (c) Comparison of distributions predicted by (dot-dash/blue line) the stochastic individual model, (Ia), (dashed/red line) the mesoscopic velocity-jump model, (Ib), and (solid/black line) the macroscopic model, (II). Distributions plotted as functions y, averaged over x; distributions for the individual model are the mean of 1000 simulations. Frames (top to bottom) are for $t = 10, 100, 1000$ at the various speeds indicated at the top of each column. Other model parameters set at $\tau = \kappa = 1 = E_0 = y_0 = L_x = 1$, $L_y = 2$ and $a = 10$. For details of the numerical methods we refer to the appendix.

Even when the macroscopic model breaks down, the mesoscopic velocity-jump model remains valid and can be employed if a continuous approach is required. Of course, this is also subject to caveats: this correspondence can only be expected under the assumed independence of individuals, and we refer to the discussion for further consideration of this potentially important case.

3 Hilltopping dynamics in butterflies

The above provides a mechanistic framework for moving between individual-level and population-level modelling of movement under various spatio-temporal orienteering cues. For the remainder of this paper we focus on the main application: the impact of hilltopping on mating in butterflies. As noted earlier, in hilltopping it is the local terrain that provides the orienteering cue for movement, with individuals flying up slopes to local summits.

This application is motivated both from a basic illustrative aim as well as addressing fundamental questions concerning hilltopping. Long-term studies have resulted in a large pool of data on butterfly population dynamics and their fluctuations under environmental pressures, producing a model system for determining the robustness of populations (Ehrlich and Hanski 2004). The mechanisms that facilitate mating encounters, such as hilltopping, are therefore of manifest interest and a variety of studies have specifically focussed on its impact, for example see Shields (1967); Scott (1968); Ehrlich and Wheye (1986); Alcock (1987); Baughman et al. (1988); Wickman (1988); Turchin et al. (1991); Pe'er et al. (2004). With regards to modelling, these researches provide the data to inform a mechanistic model for the dynamics of a virtual hilltopping population.

In the following we formulate a series of models from individual to macroscopic and explore how hilltopping impacts on butterfly population structure. We first replicate typical flight paths for a population in topologically complex environments, explore convergence between models and, by incorporating simple kinetics, determine how hilltopping impacts on mating.

3.1 Basic movement models

3.1.1 Environment and population details

As previously mentioned, butterflies generally remain close to the ground and we restrict their flight movements to a two-dimensional square landscape A of dimensions $L \times L$, setting $(x, y) \in A \subset \mathbb{R}^2$ as the spatial coordinate; for all simulations here we consider $L = 2$ km. While butterflies receive a wide variety of movement cues from their environment (e.g. Dover and Settele 2009), here we fix attention on topography as the principal orienteering cue. Specifically, we assume all guidance information is stored in the (fixed) elevation of the imposed landscape, $E(x, y)$ (measured in metres).

We consider a range of terrains, ranging from artificial to genuine. The former are generated through a linear combination of 2D Gaussian functions as follows:

$$E(x, y) = \sum_{i=0}^{K} h_i e^{-\frac{(x-x_i)^2 + (y-y_i)^2}{2\sigma_i^2}} . \tag{13}$$

Setting $h_0 > 0$, $h_i = 0$ for $i > 0$ and $x_i = y_i = L/2$ generates the *ideal landscape* of a perfectly circular hill, centred in A: see Figure 3(a). Combining multiple Gaussian functions can generate more complicated topography, such as the *undulating landscape* in Figure 3(b). For the *genuine landscape* we digitise the terrain centred on Arthur's Seat, a peak rising to approximately 250 metres near the centre of Edinburgh: Figure 3 (c) indicates the topography at this site. For comparative purposes, all artificial landscapes are normalised such that the maximum elevation gain across A is 200 metres, approximately the same as that of the terrain surrounding Arthur's Seat.

Simulations are performed for time $t \in [0, T]$, where T denotes either the time butterflies are studied or the overall length of a flight season. Outputs from simulations will often be represented in days or weeks, however we note that one day corresponds to just T_{active} hours in model simulation time, since butterflies are assumed active for only a portion of a day. For simulations here we set $T_{active} = 10$ hours; generally, T_{active} will be species, climate and habitat dependent, e.g. Kingsolver (1983).

Models explicitly consider *males* (m) and *virgin females* (f); we ignore mated females, assuming they have no explicit impact on population dynamics and exit to lay eggs following copulation. Note that the location of egg laying may be an important input in terms of sources of new butterfly emergence: suitable vegetation for eggs (and caterpillars) can be sparsely distributed and away from exposed hilltops, for example see Ehrlich and Hanski (2004). Initially we ignore explicit
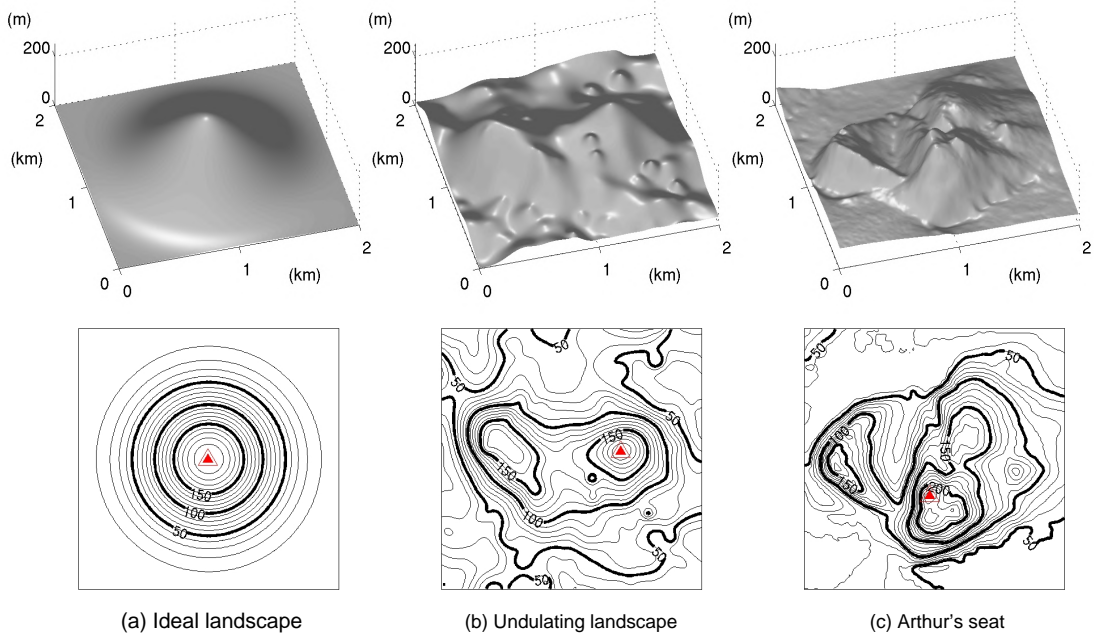
Fig. 3 Landscapes used for simulations. Top panels show the relief, with height depicted in metres and (x, y) coordinates in kilometres; bottom panels show contour lines, with thin contours representing 10 m intervals and thicker contours indicating 50 m intervals. The highest point in each landscape is marked with a triangle. (a-b) Artificial terrains showing (a) an ideal hill, and (b) an undulating landscape: see text for details. (c) Terrain surrounding Arthur's Seat (Edinburgh, UK, $55°56'N, 3°09'W$). Elevation data obtained using OS Opendata Land-Form PANORAMA (http://www.ordnancesurvey.co.uk/oswebsite/).

descriptions of population dynamics (emergence, mating and death): our first simulations form an idealised mark-release-recapture study in which a population is released into an empty (of butterflies) landscape, with the study-time sufficiently short that population dynamics can reasonably be ignored. This allows us to focus on definitions of the movement response to terrain, demonstrate hilltopping and explore model convergence.

3.1.2 Modelling flight paths

Noting the earlier considerations, individual butterfly flight paths are modelled according to the simplified stochastic jump process in Section 2.2, in which turns occur with constant mean frequency into a new velocity direction determined by the slope/altitude. Using subscripts m and f to denote the distinct flight characteristics of males and virgin females, we define $\tau_{m,f}$ to be the mean flight-times between turning/landing, $s_{m,f}$ as the mean flight speeds and $q_{m,f}$ to be the probability distribution for turning into velocity $\mathbf{v}_{m,f} = s_{m,f}(\cos\theta, \sin\theta)$. As mentioned earlier, the latter can be restated as directional distributions, $\tilde{q}_{m,f}(\theta) \equiv q_{m,f}(\mathbf{v})/s_{m,f}$ to turn into angle θ. The corresponding movement-only mesoscopic velocity-jump model for the butterflies is given by

$$p_{m_t}(t, x, y, \mathbf{v}) + \nabla \cdot \mathbf{v} p_m(t, x, y, \mathbf{v}) = \frac{m(t, x, y)q_m(x, y, \mathbf{v}) - p_m(t, x, y, \mathbf{v})}{\tau_m}, \tag{14a}$$

$$p_{f_t}(t, x, y, \mathbf{v}) + \nabla \cdot \mathbf{v} p_f(t, x, y, \mathbf{v}) = \frac{f(t, x, y)q_f(x, y, \mathbf{v}) - p_f(t, x, y, \mathbf{v})}{\tau_f}. \tag{14b}$$

In the above, $p_{m,f}(t, x, y, \mathbf{v})$ define the densities of male and female butterflies moving with velocity $\mathbf{v}$, while $m(t, x, y)$ and $f(t, x, y)$ denote the corresponding macroscopic densities. The subscript t denotes the partial time derivative. Scaling as in Section 2.3 generates the macroscopic model:

$$m_t + \nabla \cdot (\mathbf{a}_m m) = \nabla\nabla(\bar{D}_m m) \,; \tag{15a}$$

$$f_t + \nabla \cdot (\mathbf{a}_f f) = \nabla\nabla(\bar{D}_f f) \,. \tag{15b}$$

$\mathbf{a}_{m,f}$ and $\bar{D}_{m,f}$ are the previously defined drift-velocities and anisotropic diffusion tensors, computed according to $q_{m,f}(x, y, \mathbf{v})$ through (6)–(7).

3.1.3 Initial and Boundary Conditions

The first investigation ignore resident populations and assume a total of N released butterflies (N_{rm} males and N_{rf} virgin females) in a simulated mark-release-recapture study. For the stochastic model, we select the initial position of the (i^{th}) male butterfly from a circular bivariate normal distribution (centred on $(x_{i,ic}, y_{i,ic})$ and with spread σ_i), while initial velocities are selected from a uniform distribution. Translated to the continuous models, this generates initial conditions in the form of sums of 2D Gaussian functions:

$$p_{m0}(x, y, \mathbf{v}) = \sum_{i=1}^{N_{rm}} \frac{1}{2\pi} \frac{1}{2\pi\sigma_i^2} e^{-\frac{(x-x_{i,ic})^2 + (y-y_{i,ic})^2}{2\sigma_i^2}} \,;$$

$$m_0(x, y) = \sum_{i=1}^{N_{rm}} \frac{1}{2\pi\sigma_i^2} e^{-\frac{(x-x_{i,ic})^2 + (y-y_{i,ic})^2}{2\sigma_i^2}} \,.$$

Note that equivalent forms will be generated for the females. At the boundaries of A we consider the same no-loss conditions as in the earlier case studies.

3.1.4 Turning responses

Orientation in response to the landscape is to be encoded into the turning distribution, as considered in Section 2.4. Note that here we will restrict to a time-independent turning distribution: in practice, visits to mating encounter-sites such as hilltops can be confined to certain hours of the day (Rutowski 1991), and a time-dependent turning distribution may therefore be more realistic for certain species. Since field studies of hilltopping butterflies indicate their tendency to choose an upward slope (Turchin et al. 1991; Pe'er 2003; Pe'er et al. 2004), we follow the modelling choices of the earlier case study: we assume the unidirectional von Mises form (8), with $\phi(x, y)$ and $k(x, y)$ determined by the gradient of $E(x, y)$. Specifically, we set angle $\phi(x, y)$ in the direction of the gradient $\nabla E(x, y)$ and $k(x, y)$ according to its steepness: $k_{m,f}(x, y) = \kappa_{m,f} |\nabla E(x, y)|$. Hence

$$q_{m,f}(x, y, \mathbf{v}) = \frac{\tilde{q}_{m,f}(x, y, \theta)}{s} \,, \text{ where } \tilde{q}_{m,f}(x, y, \theta) = \frac{e^{\kappa_{m,f} |\nabla E(x,y)| \cos(\theta - \phi(x,y))}}{2\pi I_0(\kappa_{m,f} |\nabla E(x,y)|)} \,. \tag{16}$$

Thus, the tendency to fly uphill increases with steepness. The parameter $\kappa_{m,f}$ defines the *hilltopping tendency* of the population: $\kappa_{m,f} = 0$ corresponds to a non-hilltopping population while large $\kappa_{m,f}$ indicate a strong tendency to fly up slopes. Certain populations may possess exquisite sensitivity to topography, with field studies indicating accumulation of individuals at the maxima of quasi-flat terrains (Baughman and Murphy 1988). With the von Mises form (8), explicit calculations for the functions $\mathbf{a}_{m,f}$ and $\bar{D}_{m,f}$ in Equations (15) are directly computed from $E(x, y)$ via (9)–(10), i.e. elevation data directly feeds into the movement terms of the macroscopic model.

Set	Parameter	Definition	Units	Value/range
Flight	$s_{m,f}$	Mean flight speed	metres/minute	2.5
Flight	$\tau_{m,f}$	Mean run time	minutes	2 (m), 4 (f)
Flight	$\kappa_{m,f}$	Hilltopping tendency	(none)	0 - 20
Kinetics	$\delta_{m,f}$	Death rate	/week	1.0
Kinetics	β	Mating rate	/butterfly/hectare/hour	0.005
Kinetics	α	Emergence rate	/hectare/week	1-1000

Table 1 Model parameters used in simulations.

In fact, tracking studies in Pe'er et al. (2004) indicate a more sophisticated response than simple local gradient detection: butterflies in the vicinity of multiple peaks typically select the highest within visual range (approximately 50 metres). A future extension would be to evaluate the consequences of different slope-following strategies, via appropriate sampling of their surrounding environment.

3.1.5 Parametrisation

The various model elements (release location, flight characteristics, terrain elevation *etc.*) generate a sizeable parameter set and systematic exploration of the full space is unrealistic. Therefore, we utilise established datasets (from tracking) to fix certain parameters and estimate ranges. Field studies of *Melitaea trivia* (Pe'er 2003; Pe'er et al. 2004) provide a set of estimates for $s_{m,f}$ and $\tau_{m,f}$; parameters for other species are likely to differ, with a corresponding impact on the spatial and temporal scales of dispersal. Release locations will be specified in individual simulations.

Instantaneous butterfly flight speeds will typically be several kilometres per hour (e.g. Pe'er 2003; Cant et al. 2005), however over a longer timescale a butterfly is likely to spend a considerable proportion of time involved in other activities (resting, feeding). As previously noted, one approach would be to explicitly account for this via splitting the population into flying and resting subpopulations (e.g. see Othmer et al. 1988; Hillen 2003), however we presently ignore such complications. Rather, we consider for the flight speed a value averaged over a much longer flight path, taking a value towards the lower end of the spectrum reported in Pe'er (2003) and setting $s_{m,f}$ to be 2.5 metres/minute. Consequently, paths generated here should not be strictly viewed as true depictions of butterfly flight, rather an 'effective path' traced out. With these speeds, and the reported mean distances between turning points determined as approximately 5 metres for males and 10 metres for virgin females (Pe'er et al. 2004), we take mean flight times $\tau_m = 2$ and $\tau_f = 4$ minutes.

$\kappa_{m,f}$ are the key parameters that define the hilltopping tendency, and we leave this unspecified to evaluate its impact on population organisation. While studies in Pe'er et al. (2004) indicate a greater tendency of virgin females of *Melitaea trivia* to climb slopes ($\kappa_f \geq \kappa_m$), here we restrict to $\kappa_f = \kappa_m$. The set of *flight parameters* is recorded in Table 1. We note that the differences between male and female flight parameters is small, and studies (not shown) with identical parameters will generate similar results. Nevertheless, we retain the distinct flight characteristics for realism, with a more detailed exploration into the impact of distinct characteristics planned for future studies.

3.2 Hilltopping studies

We first perform a simulated tracking study for a population released into various landscapes: specifically, butterflies are released at a particular location and their subsequent flight paths are tracked, discretised according to the turning locations. We exploit the capacity of modelling to

focus on specific phenomena, concentrating on the oriented movements that lead to hilltopping behaviour. We assume the released population is homogeneous (male only, with identical movement properties) and that the environment is otherwise devoid of butterflies. We note that simulations for females generate (qualitatively) equivalent behaviour to those for males shown below. We will demonstrate how the individual model captures the directed movement observed in field studies (e.g. Turchin et al. 1991; Pe'er et al. 2004), explore its capacity to replicate hilltopping and the extent to which the individual model converges with the continuous mesoscopic and macroscopic models.

3.2.1 Hilltopping in the individual model

Individual butterflies are released into a landscape of constant gradient, sloping upward in the direction of increasing x: hilltopping would be characterised by a tendency to fly rightwards. We simulate the stochastic individual-based model, releasing (at $(0,0)$) and tracking 100 butterflies (male-only with hilltopping tendency $\kappa_m = 5$). Figure 4 (a)-(d) plots representative trajectories and the collected statistics for populations released on slopes of varying steepness. We plot frequency histograms for the orientation taken at a turning location (where $0°$ corresponds to the angle directly uphill) and the runtime between turning points.

Hilltopping is clearly observed, demonstrated through a shift from an unbiased random walk for flat terrains (Figure 4 (a)) to a highly biased path uphill on a steep slope (Figure 4 (d)). The simplified form of the model is reflected in the frequency distributions: while the angle of orientation becomes increasingly concentrated into an uphill direction with steeper slopes, the runtime remains unaltered (exponentially distributed with the mean value listed in Table 1). Figure 4 (e)-(g) evaluates hilltopping tendency as a function of the slope through the following statistics: (e) the mean displacement uphill (i.e. the average position of a butterfly along the x-axis after 10 hours); (f) the mean first transit time (the average time at which a butterfly first crosses a transect located 500 metres uphill from the release location); and (g) the mean turning angle (i.e. the angular difference in orientation between consecutive runs). The displacement and first transit times increase and decrease respectively, saturating towards the maximum displacement (mean flight speed $\times$ 10 hours) and minimum transit time (500/mean flight speed). The mean turning angle decreases towards zero, reflecting an increased persistence of butterflies in the same direction, i.e. in uphill directions.

While the above simulations are for fixed flight parameters, the impact of varying these parameters is as intuitively expected: increasing κ has the same effect as increasing the slope and, while altering mean flight speed and turning rates changes the mean displacement, transit times *etc.*, it does not impact on the overall hilltopping behaviour.

3.2.2 Model comparison

We next consider an imposed landscape: the ideal hill centred in A, see Figure 3 (a). As above, we consider the release of a homogeneous (male) population with flight parameters as in Table 1. Representative simulations of the individual-based model are plotted in Figure 5 (a) for various hilltopping tendencies κ_m. Each butterfly is released approximately 1 km from the summit and their flight path is tracked either until they reach within 100 m of the summit, or 100 hours (10 days) of flight time has passed. Increasing κ_m corresponds to a greater capacity to summit, reflected in more individuals reaching the summit (within 10 days), straighter paths and a decrease in the time taken.

This idealised study is exploited to explore model correspondence and the validity of a macroscopic approximation. We numerically solve (14) and (15) under equivalent release, terrain and flight conditions and compare against average distributions obtained from multiple simulations of
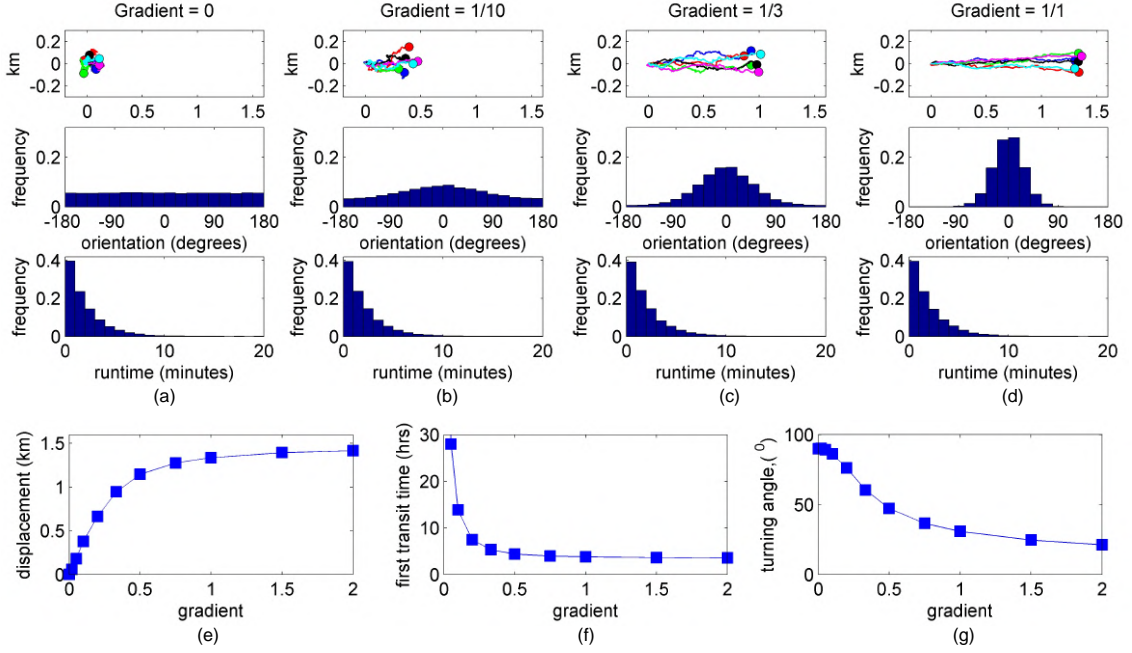
Fig. 4 Individual paths computed by the individual-based model. 100 identical butterflies are released at point $(0, 0)$ and tracked over a period of 10 hours: for these simulations, we take the male flight parameters from Table 1 and $\kappa_m = 5$. Simulations are performed on slopes of varying gradient: (a) zero gradient (flat terrain); (b) 1:10 gradient (inclination angle $5.71°$); (c) 1:3 gradient ($18.43°$); (d) 1:1 gradient ($45°$). For each we plot (from top to bottom) representative flight paths, the orientation histogram (with $0°$ indicating rightwards), and the histogram of flight times between turning/landing. (e-g) Population averaged behaviour as a function of the gradient showing: (e) the mean displacement uphill; (f) the mean first transit time; (g) the mean turning angle between successive flights. For details of the simulation method, we refer to the appendix.

the individual model. From the earlier case study we expect that the mesoscopic velocity-jump model matches the mean behaviour of the individual model, with (15) also comparable if the scale is macroscopic. Figure 5 (b) summarises the results: in the first row we plot the averaged (over 1000 simulations) population distribution (blue to red indicates low to high densities) predicted by the individual model at various times, following the initial release of 100 hilltopping butterflies ($\kappa_m = 5$) at a site located 1 km from the summit; second and third rows respectively plot the distributions generated by the mesoscopic and macroscopic models. We observe a quasi-identical match, exemplified in the bottom row plot for the distributions along the diagonal transect. Further studies for distinct, yet plausible, parameter sets or with different terrains corroborate this similarity.

Firstly, this investigation confirms the scaling: correspondence between the models is observed, validating the macroscopic terms and parameter calculations. Secondly, they indicate that populations dynamics can be adequately approximated by the macroscopic model. We will therefore exploit its greater tractability (both analytical and numerical) over the intermediate mesoscopic model, dispensing of the latter in subsequent investigations. Note, however, that other applications may demand employment of the mesoscopic model, if relevant and important features of the population dynamics are lost due to the scaling.
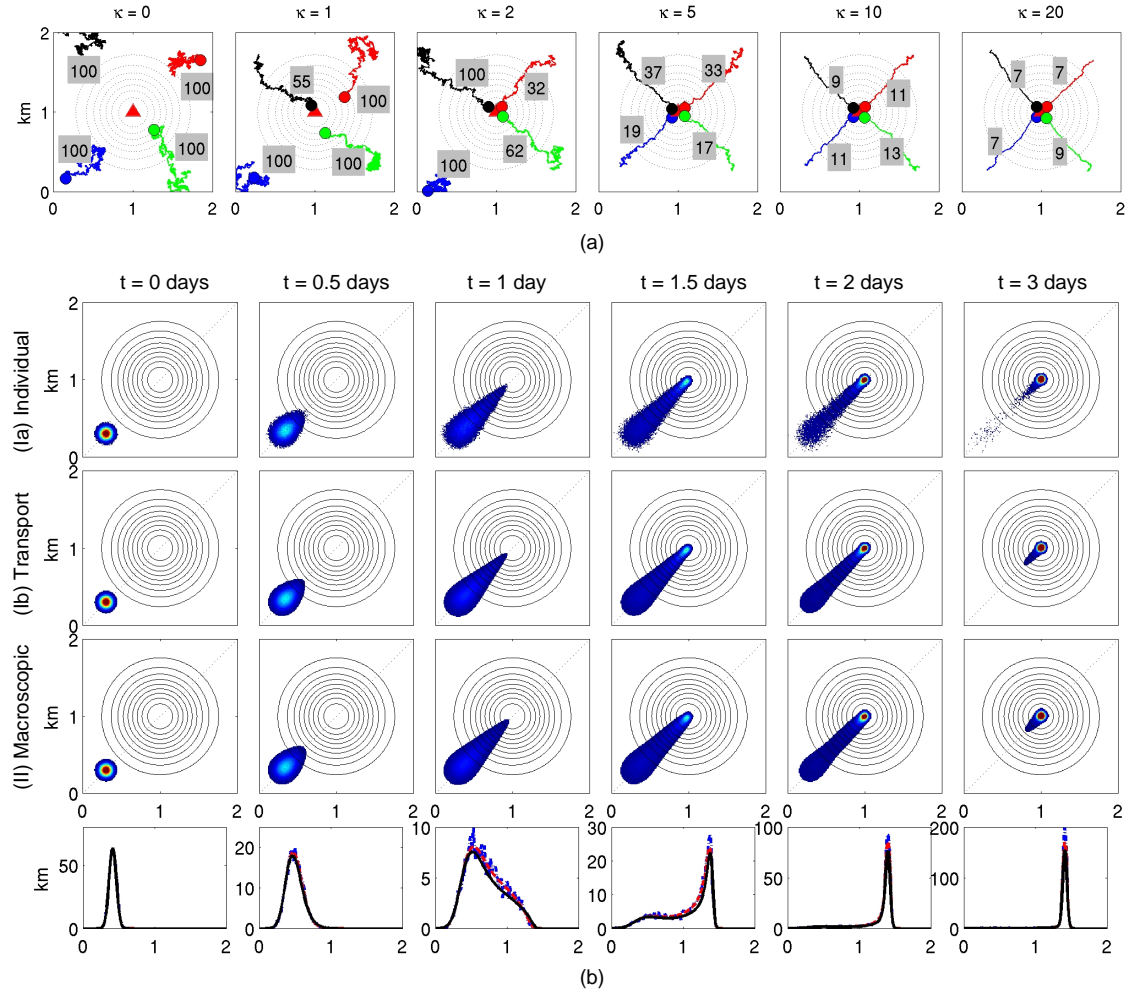
(a)

(b)

Fig. 5 Hilltopping and model comparison for an ideal hill. (a) We show 4 representative trajectories of butterflies released into the ideal hill environment: frames from left to right are for increasing values of κ. Each butterfly starts approximately 1 km from the summit and is tracked either until it arrives within 100 metres of the summit or 100 flight hours (10 days) have passed. The final location of a butterfly is shown by the circle, with the number of flight hours for each trajectory indicated in the highlighted text. (b) Comparison of density distributions generated for (first row) the stochastic individual-based model, (second row) the mesoscopic velocity-jump model and (third row) the macroscopic model. Density distributions plotted at times indicated at the top of the panels, following the initial release of 100 individuals at a site centred 1 km from the summit. White shaded regions indicate ≤ 0.01 butterflies/hectare, with blue to red representing an increasing butterfly density (dark red $= \geq 50$ butterflies/hectare). In the bottom row we plot the density (in butterflies/hectare) along the diagonal transect: dot-dash and blue line = individual-based model, dashed and red line = mesoscopic model, solid and black line = macroscopic model. Coordinate axes denoted in km. Parameters and model details as in text. For details of the numerical methods, we refer to the appendix.
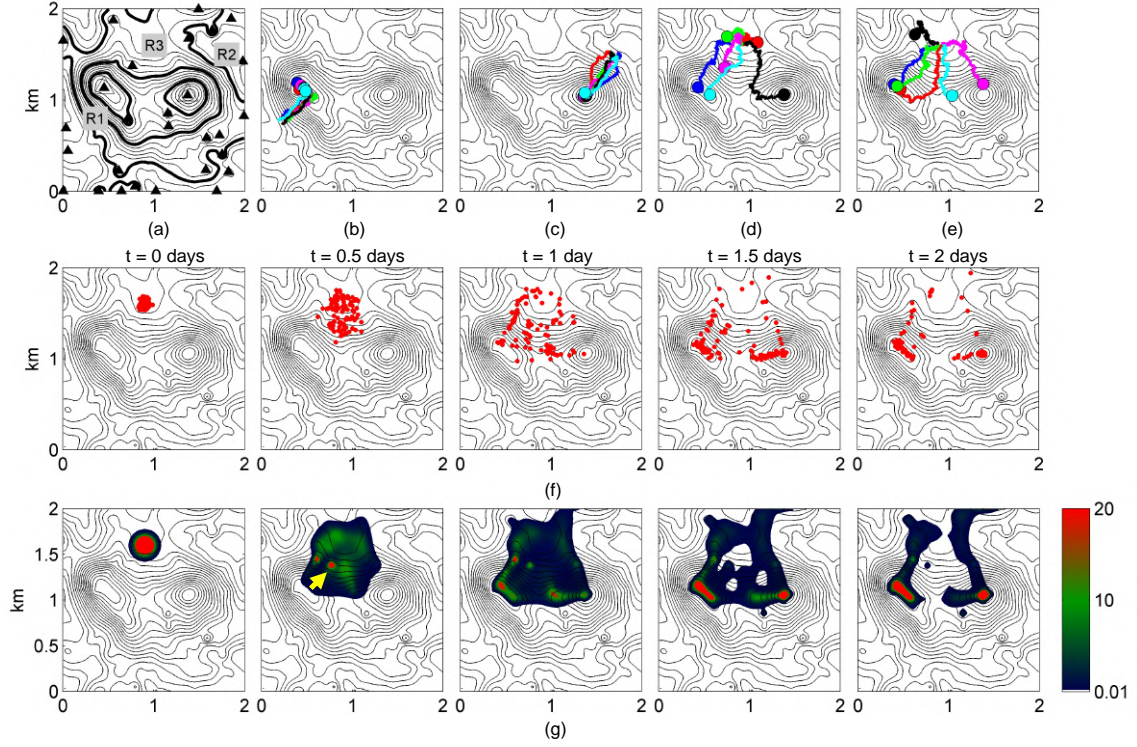
Fig. 6 Hilltopping in a complex terrain. (a) Illustration of the site topography, with all peaks marked with a triangle and the two major peaks marked with the double triangles. The three release sites are indicated R1-R3. (b-c) Individuals released from either site (R1) or (R2) nearly always fly directly uphill to the nearest of the two major peaks. (d-e) Individuals released from site (R3) show greater variability in their movement, either flying to one of the main peaks or meandering at lower level and visiting minor peaks. (f-g) Comparison between distributions predicted by the (f) individual-based model and (g) macroscopic model (15). Colorscale to the right of (g) indicates the butterfly density, in butterflies/hectare. In these simulations, 100 individuals are released from site R3. Note that temporary accumulations occur at intermediate peaks *en route* to the major peaks, for example as indicated by the arrow at 0.5 days. Parameter details as described in the text, numerical details described in the appendix.

3.2.3 Complex terrains

The final part in our initial investigation explores movement dynamics for butterflies released into a more complex terrain. Figure 6 (a) reveals the contour profile of the landscape and release sites. We consider three locations, (R1)-(R3), and release 100 hilltopping ($\kappa_m = 5$, male-only) butterflies with flight parameters as in Table 1. Paths are tracked for a total of 2 days (20 hours flight time). Individuals released at (R1) or (R2) typically move directly uphill, accumulating at the nearest of the two major peaks to their release location: representative trajectories are plotted in Figure 6 (b) and (c) respectively. The consistency of trajectories echoes the findings of Pe'er et al. (2005) in a similar modelling study: topography funnels the trajectories along 'virtual corridors'. Flight paths for releases from site (R3), located further down slope and in a flatter region, show greater variability: individuals move towards and localise at different peaks, e.g. Figure 6 (d-e).

To explore the subsequent population distribution we plot (f) the locations of all released individuals at distinct times and (g) the population distribution computed from the fully macroscopic model; note that the latter distribution closely matches the averaged distribution from multiple simulations of the individual model, as expected from the investigation above. This study reveals

that the population splits into two factions respectively moving towards one of the two major peaks, although a small fraction remains at lower elevations. Note also that intermediate accumulations can occur at lower-level peaks, e.g. the yellow arrowheads at $t = 1$ day: these lower peaks may provide an intermediate rendezvous location.

4 Impact of hilltopping on mating

Hilltopping is generally regarded as a mechanism to increase encounter rates, and we expand the investigation to explore its impact on mating. Given its capacity to quantitatively predict distributions of the underlying individual model, we focus exclusively on the macroscopic model, exploiting the ease with which it can be augmented with classical population kinetics:

$$m_t + \nabla \cdot \mathbf{a}_m m = \nabla\nabla(\bar{D}_m m) + g_m(t, x, y) - \delta_m m \, ; \tag{17a}$$

$$f_t + \nabla \cdot \mathbf{a}_f f = \nabla\nabla(\bar{D}_f f) + g_f(t, x, y) - \beta m f - \delta_f m \, . \tag{17b}$$

The emergence of new butterflies from pupae is assumed to take place at rates $g_{m,f}(t, x, y)$: generally these will be position- and time-dependent functions to reflect a heterogeneous and variable emergence rate across the course of a season (Iwasa et al. 1983). $\delta_{m,f}$ define the (assumed linear) death rates. In the above equations mating is modelled as an 'encounter' similar to standard disease modelling: we assume a loss of virgin females at a rate proportional to the local male and virgin female densities, with mating encounter rate β. For the simplified model here, males are allowed to have unlimited mating potential whereas females mate just once before exiting to lay eggs: males usually mate more often than females (e.g. see Scott 1973b), although potency may diminish with age and females of certain species may also mate multiple times; future extensions of the model may relax the specific assumptions here. As previously, we study the dynamics of (17) for $t \in [0, T]$, where T denotes either the time butterflies are tracked or the overall length of a flight season, and $(x, y) \in A$, where A is one of the landscapes featured in Figure 3.

For presentation purposes we track both the *cumulative density distribution of mating events* (at time t), $\int_0^t \beta m(x, y, \tau) f(x, y, \tau) d\tau$, and the *total number of matings* (at time t), $\int_0^t \int_A \beta m(x, y, \tau) f(x, y, \tau) dA d\tau$. The former generates a density map of how many and where matings have taken place by time t, with the latter tracking the total number of matings across the studied region by time t.

4.1 Parametrisation, initial and boundary conditions

4.1.1 Parameters

Any parametrisation of (17) must be taken with caution: in addition to the distinct flight characteristics, emergence, death and mating rates are highly variable with species, habitat, weather, *etc.* In particular, emergence rates are dependent on conditions (e.g. climatic) during the current and previous years: population densities can fluctuate widely over the years, varying by several orders of magnitude (Hellmann et al. 2003). For low density species (or low density years), increasing one's chance of mating is likely to impact more heavily on overall population dynamics and, to investigate this potentially crucial dependence, we take a pragmatic approach to parametrisation: we fix mating and death rates at estimated values and allow the emerging numbers to vary over a broad range, thus generating a spectrum of population sizes through single parameter variation. Additional data would allow a more precise, species-specific investigation to be conducted.

We define the parameters $N_{em}(= \int_0^T \int_A g_m(x, y, t) dA dt)$ and $N_{ef}(= \int_0^T \int_A g_f(x, y, t) dA dt)$ as the total numbers of emerged males and females, respectively. Butterflies are typically assumed to

emerge in a 1 : 1 ratio, as holds under many laboratory-controlled studies, although the extent to which this holds true in the field will be dependent on a variety of factors (e.g. see Ehrlich et al. 1984). For example, infections by the *Wolbachia* bacteria can lead to grossly distorted sex ratios for certain species, e.g. Jiggins et al. (2000). Here we strictly assume the 1 : 1 ratio holds, i.e. $N_{em} = N_{ef}$, and leave any investigation of unequal emergence for future studies.

To parametrise death rates we assume a mean lifespan for a butterfly to be one week: lifespans vary considerably across species (from as little as a day to about a year), however one week appears a reasonable approximation for many hilltopping species (e.g. Scott 1973a). Note that estimates in reared/protected butterflies can be distinct to their wild counterparts, due to differences in vulnerability to infections, weather conditions, predation (e.g. birds, see Bowers et al. 1985), etc. While distinct behaviours may lead to distinct death rates for males and females, we ignore such complications at present and assume $\delta_m = \delta_f = 1.0$ per week. Note that the modelling implicitly assumes no nonlinearities in the death rate, such as higher predator numbers at points where butterflies accumulate.

The mating rate will also depend on factors such as the ability to detect a mate and the length of courtship/copulation (Scott 1973b). We exclude any complexities, such that mating only takes place during certain hours, or that butterflies only gain reproductive potential at a certain age following emergence, and simply take the mating rate to be uniform and constant. We set $\beta = 0.005$ per males/hectare per hour: this assumes that the mean time for a virgin female to mate in a terrain containing male butterflies at a mean density 100/hectare is 2 hours. We finally remark that the simulation study below has also been conducted for other feasible mating/death rate parameters, with the same qualitative behaviour observed. The set of *population kinetic parameters* used is listed in Table 1.

4.1.2 Initial and boundary conditions

Our model studies will be conducted according to one of two situations.

(i) *Controlled mark-release-recapture study.* We assume released populations of sizes N_{rm} and N_{rf} for males and females, respectively, and no resident population ($N_{em} = N_{ef} = 0$). Here, $t = 0$ indicates the release time and $t = T_{study}$ denotes the end of the study period.

(ii) *Natural emergence over a flight season.* We assume $N_{em} = N_{ef} > 0$ and no initial (or released) population, $N_{rm} = N_{rf} = 0$. Here, $t = 0$ indicates the beginning of the flight season and $t = T_{season}$ indicates the season length.

For (i) we initially assume released males and females are concentrated at separate sites according to 2D Gaussian functions:

$$m_0(x, y) = N_{rm} \frac{e^{-((x-x_{m,ic})^2 + (y-y_{m,ic})^2)/2\sigma_m^2}}{2\pi\sigma_m^2},$$

$$f_0(x, y) = N_{rf} \frac{e^{-((x-x_{f,ic})^2 + (y-y_{f,ic})^2)/2\sigma_f^2}}{2\pi\sigma_f^2},$$

where $(x_{m,ic}, y_{m,ic})$ and $(x_{f,ic}, y_{f,ic})$ respectively describe the male and female release locations, with $\sigma_{m,f}$ denoting the spread about these sites. For (ii) we simply set $m_0(x, y) = f_0(x, y) = 0$. As previously, we assume no loss or gain of butterflies across the edges of the study field, imposing zero-flux boundary conditions on (17).
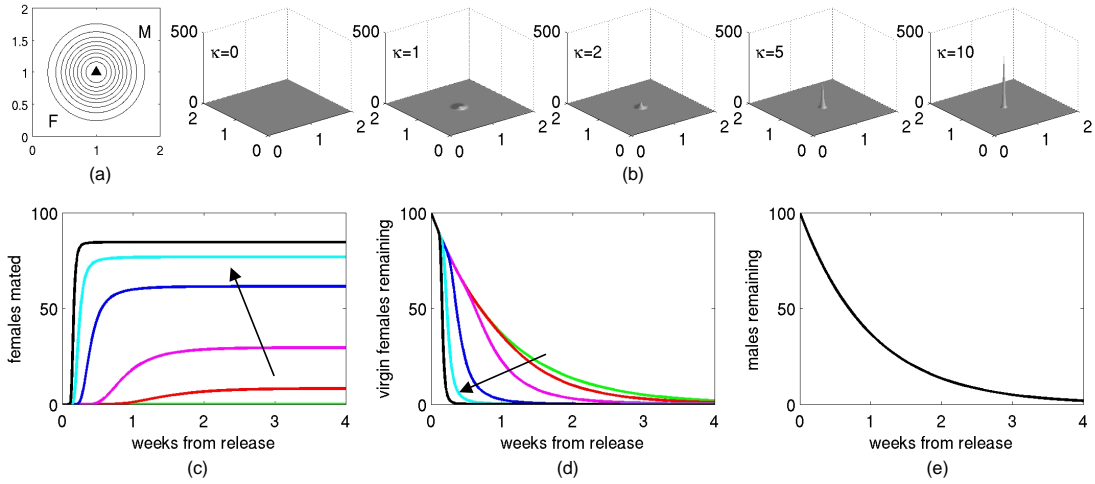
Fig. 7 Impact of hilltopping on the mating efficiency of a butterfly population. (a) 100 male and 100 female butterflies were released at $t = 0$ at the 2 sites indicated, separated by 2 km on opposite sides of the ideal hill. (b) The accumulated distribution of matings across the field after 4 weeks, for increasing values of κ: matings are confined to the summit and rise with greater hilltopping tendency; horizontal axes indicate location, vertical axis indicate the accumulated density in matings/hectare. (c) Number of females that have mated as a function of time (the arrow indicate results under increasing κ). (d-e) Remaining number of (d) virgin females and (e) males for increasing κ. In (c-e) we have (green) $\kappa = 0$, (red) $\kappa = 1$, (magenta) $\kappa = 2$, (blue) $\kappa = 5$, (cyan) $\kappa = 10$ and (black) $\kappa = 20$. For model and parameter details we refer to the text, for details of numerical methods we refer to the appendix.

4.2 Mark-release-recapture studies

Our first study exploits the controlled nature of a mark-release-recapture style study. Specifically, we consider the separated releases of males and virgin females as described above and track the subsequent population dynamics. Here we assume $N_{rm} = N_{rf} = 100$. We set $T_{study} = 4$ weeks, noting that very few butterflies remain (see Figure 7 (d-e)) at the end of the study.

In the first investigation we consider the ideal hill, Figure 3 (a). We release the male and female populations on opposite sides of the summit, separated by 2 km: see Figure 7 (a). In each case we assume males and females have an identical capacity to hilltop, $\kappa_m = \kappa_f = \kappa$, and increase κ between 0 and 20 to consider populations with distinct tendencies. Results are summarised in Figure 7 (b)-(e), where we plot: (b) the cumulative density distribution of mating events after 4 weeks; (c) the % of females that successfully mate; (d) the percentage of remaining virgin females; and (e) the percentage of remaining males. Note that the last is unaltered with κ: male loss is a result of natural death only and the population decays exponentially according to the death rate.

Clearly, mating is significantly assisted by hilltopping, with the % of mated females rising with an increased tendency to hilltop. For $\kappa = 0$ (i.e. no hilltopping) the initial separation is too large, precluding random encounters between males and females: the number of matings is insignificant. At lower values of κ the summit draws males and virgin females together to mate, however its weak nature results in a significant number of females dying before encountering a male. As κ is increased, individuals will take a more or less direct route to the summit (e.g. see Figure 5 (a)) and subsequently a high percentage of females mate. The cumulative density distribution of mating events after 4 weeks shows a concentration of matings at the summit, with maximum concentrations at the highest values of κ.

4.3 Seasonal dynamics

We next consider the mating dynamics for a naturally emerging population over the course of a flight season. Specifically, we assume butterflies begin to emerge at time $t = 0$ (the start of the season) and track distributions until $t = T_{season}$; we take $T_{season} = 8$ weeks. We assume no prior (or released) populations, i.e. $m_0(x, y) = f_0(x, y) = 0$.

Realistically, emergence functions g_m and g_f will be both spatially heterogeneous and time dependent: the spatial pattern of emergence will be localised according to larval food vegetation, while the timing is typically weighted towards the start of the mating season (e.g. Iwasa et al. 1983). Moreover, discrepancies occur between males and females, with the former usually emerging a few days earlier (Iwasa et al. 1983). To exclude any environmental induced heterogeneity (beyond hilltopping movement), we suppose emergence, and hence larval vegetation, is uniformly distributed across the region. Further, we restrict time-emergence to a simple step-function form such that emergences occur at a uniform rate in a 1:1 relationship over the first four weeks:

$$g_{m,f}(t, x, y) = \begin{cases} \alpha/2 & \text{if } t \leq 4 \text{ weeks} \\ 0 & \text{if } t > 4 \text{ weeks} \end{cases},$$

where α defines the emergence rate of all butterflies, measured in butterflies/hectare/week.

To understand the extent to which hilltopping benefits species/populations of distinct sizes, we classify the following four population sizes according to the emergence rate α:

– *Rare*, $\alpha = 1$ (total population/hectare $= 4$);
– *Low*, $\alpha = 10$ (total population/hectare $= 40$);
– *Average*, $\alpha = 100$ (total population/hectare $N = 400$);
– *Abundant*, $\alpha = 1000$ (total population/hectare $N = 4000$).

Hence, the population sizes studied vary across 3 orders of magnitude: such differences are not unusual amongst butterfly species, and can even occur within the same population at a particular site over different years (e.g. Hellmann et al. 2003). For each of the above populations we will explore the mating success across a range of hilltopping tendencies and landscapes; for the latter, we consider the ideal hill, the undulating landscape and the terrain surrounding Arthur's seat.

Figure 8 (a) plots the mating success of the population, defined as the % of total females that mate during the season. We note that by the end of the season all butterflies have emerged and the number of any remaining virgin females has dropped to negligible levels. In each panel we plot these percentages as a series of bar charts, as functions of the hilltopping tendency for each population size. For medium and abundant populations, hilltopping has a negligible impact on the overall mating success: densities are driven sufficiently high such that newly emerging females quickly find a mate, regardless of whether they move uphill. However, for rare and low populations, hilltopping clearly enhances mating at a population level: congregation at the summit enhances the likelihood of locating a partner and matings are frequent (with respect to the population size). In particular, we note that for the largest κ there is relatively little variation in the mating success across the distinct population sizes. Thus, hilltopping has maximum benefits for low population numbers.

We examine the spatial pattern of mating encounters for a non-hilltopping and hilltopping ($\kappa = 5$) population across the range of population sizes in Figure 8 (b). In the absence of hilltopping, encounters are uniformly distributed and range from negligible (for rare species) to frequent (for abundant species). With hilltopping, encounters are predominantly found at summits for lower density populations. However, for larger populations, matings will occur widely across the terrain and the overall number and distribution of matings is broadly consistent with that of the non-hilltopping population.
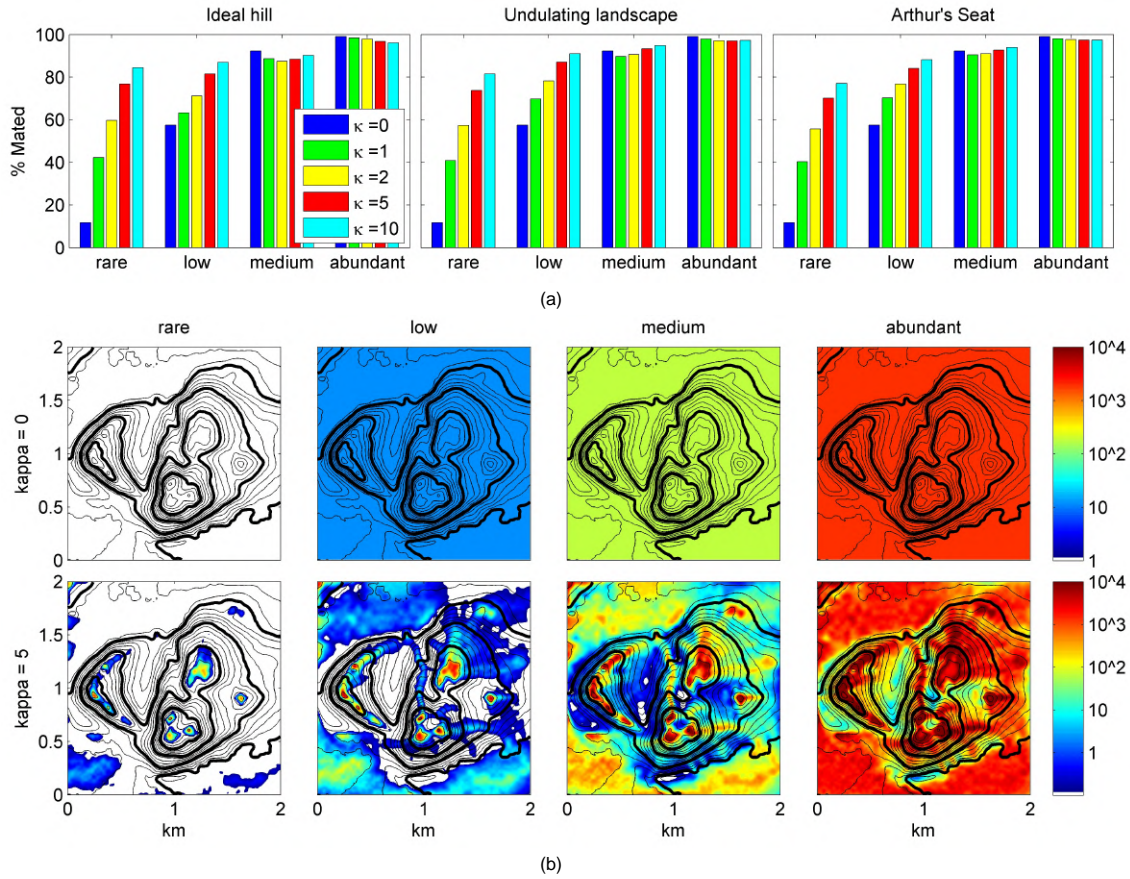
Fig. 8 Mating success for butterfly populations varying with hilltopping tendency, abundance and terrain. (a) In each frame we plot bar charts for the percentage of females that mate under distinct hilltopping tendencies (colour key in first frame) and varying population sizes (horizontal axis). Different frames show the results for different landscapes, see Figure 3. For all landscapes, a strong hilltopping strategy is shown to negate the limited likelihood of meeting a partner for low population densities. (b) Spatial plots showing the cumulative density distribution of mating encounters over the season, for various population sizes and hilltopping tendencies: results here shown for Arthur's seat terrain. Colour indicates the number of encounters/hectare according to the right-most scale. For model and parameter details we refer to the text, for details of numerical methods we refer to the appendix.

4.4 Adaptive or non-adaptive function of hilltopping

The results corroborate a long standing hypothesis: hilltopping enhances mating for rare and low density species, with summits acting as a 'lek' for males and a navigating landmark for newly emerged females (Alcock 1987). For abundant populations, any advantage gained through hilltopping is lost and mating events are dispersed across the landscape. Moreover, a non-hilltopping strategy even appears to provide a very slight advantage at a population level, with a marginally higher number of matings observed, see Figure 8 (a).

Therefore, does a male butterfly always gain by pursuing a hilltopping strategy? For abundant populations, female emergence is a relatively frequent event and, given that the majority of emergences take place away from summits, a male butterfly located at lower terrains may be better positioned to encounter and mate with a newly emerged female. Moreover, hilltops can offer a number of further disadvantages, such as greater exposure to the elements and a lack of suitable

nectar resources: blindly following a hilltopping strategy may therefore be deleterious to both an individual and the population.

We investigate this question via an extended version of (17) in which the population of males is subdivided into three phenotypes. Specifically, emerging males pursue one of three strategies: (S1) a high tendency to hilltop, $\kappa = 5$; (S2) a moderate tendency to hilltop, $\kappa = 1$; (S3) a negligible tendency to hilltop, $\kappa = 0$. Note that we will focus on distinct *male* strategies: emerging females are assumed to *always* hilltop, with the same high tendency as (S1). To exclude any further biases, we assume equal and spatially uniform emergence and death rates for all phenotypes, and that females do not show any specific predilection to mate with one phenotype over another.

Denoting $m_i(t, x, y)$ as the density of male butterflies of phenotype i, the model is extended to:

$$m_{it} + \nabla \cdot \mathbf{a}_{m_i} m_i = \nabla\nabla(\bar{D}_{m_i} m_i) + g_m(t, x, y) - \delta_m m_i \, ; \tag{18a}$$

$$f_t + \nabla \cdot \mathbf{a}_f f = \nabla\nabla(\bar{D}_f f) + g_f(t, x, y) - \sum_{i=1}^{3} \beta m_i f - \delta_f f \, . \tag{18b}$$

Note that differences in the male phenotypes arise via distinct drift velocities ($\mathbf{a}_{m_i}$) and diffusion tensors ($\bar{D}_{m_i}$), according to their hilltopping tendency. As previously, we will assume no prior butterfly populations ($m_{i_0}(x, y) = f_0(x, y) = 0$) and the following simplistic emergence functions:

$$g_m(t, x, y) = \begin{cases} \alpha/6 & \text{if } t \leq 4 \text{ weeks} \\ 0 & \text{if } t > 4 \text{ weeks} \end{cases} \quad \text{and} \quad g_f(t, x, y) = \begin{cases} \alpha/2 & \text{if } t \leq 4 \text{ weeks} \\ 0 & \text{if } t > 4 \text{ weeks} \end{cases} \, .$$

The above ensures females and (total) males emerge in a 1:1 ratio.

In Figure 9 (a) we plot the proportion of females mated according to each phenotype over the range of population sizes: the percentage stated above each chart indicates the total percentage of females that mate. In Figure 9 (b) we plot the average number of times a male of a particular phenotype mates as a function of the population size. Note that simulations are plotted using the Arthur's seat landscape: results for other terrains generate qualitatively equivalent behaviour.

For rare or low density populations, it is the (S1) males that clearly dominate the mating encounters. Here, the population densities remain low and random encounters are rare: males that have accumulated at summits are therefore most likely to encounter a female, with these males averaging more than one mating encounter. For medium population sizes, the moderate hilltopping strategy (S2) is more effective: a less tight adherence to the summit of this population offers these individuals the chance of encountering females en route to the summit. For abundant populations the behaviour observed for low density populations is completely reversed and the non-hilltopping strategy (S3) dominates. Remaining at low terrains allows these males to encounter emerging females before they start to summit.

This population-size dependency is further revealed by tracking the rate of matings according to each phenotype as a function of time as the mating season progresses, Figure 9 (b). Early in the season the hilltopping strategy is *always* more effective, regardless of the eventual population size: relatively few virgin females have emerged resulting in low densities and hilltopping co-localisation is the optimum strategy. As overall population numbers steadily increase, the hill-topping strategy loses its effectiveness and moderate or non-hilltopping strategies gain ground.

Overall, the results of this section suggest that hilltopping can be both an adaptive and non-adaptive strategy, according to overall population size, substantiating the observations in Ehrlich and Wheye (1986); Baughman and Murphy (1988).
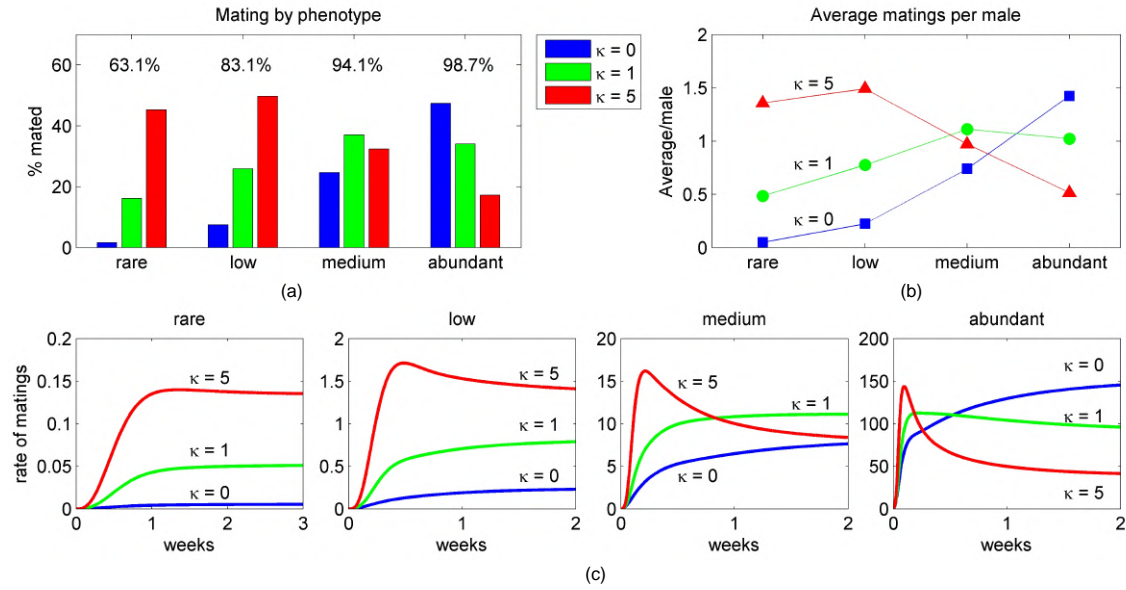
Fig. 9 Mating success of male subpopulations with distinct hilltopping tendencies. (a) % of females mated according to each phenotype expressed as bar charts, over the range of population sizes indicated along the horizontal axis. The total % of females that mate is indicated by the number above each bar chart. (b) The average number of matings per male of each subpopulation as a function of population size. (c) Rate of mating encounters by the various subpopulations during the first two weeks of the flight season, vertical axis represents matings/hectare/week. Simulations here conducted using the Arthur's seat terrain. For model details, we refer to the text, for numerical methods we refer to the appendix.

5 Discussion

A mechanistic and multiscale process for modelling oriented movements in a complex environment has been illustrated. The model is founded on a velocity-jump random walk for movement (Othmer et al. 1988, see also Codling et al. 2008; Hillen and Painter 2013; Othmer and Xue 2013), a natural description of an individual's discretised movement path. The impact of a complex environment – topography here – is accounted for via an appropriate input into the probability distribution for selecting a new orientation/velocity at a turn. If the scale is appropriate, an approximating macroscopic model for the evolution of population densities can be derived. With its computational and analytical advantages, this macroscopic model can be applied to studies of population dynamics, such as the hilltopping application considered here. At the same time, direct simulation of the underlying stochastic individual model can also be undertaken, providing an alternative viewpoint.

The velocity-jump model was tailored into a simpler and more convenient form (see also Hillen and Painter 2013) that facilitated the scaling to a macroscopic model. While the assumptions appear acceptable for the hilltopping application, they obviously limit its general applicability: as one example, the supposition that previous velocity has negligible impact on new velocities discounts that many organisms persist (even in the absence of external cues) in the same direction. Hence, applying the current scheme in a given situation must entail careful evaluation of the data and appropriateness of the assumptions. Relaxing them will require renewed consideration of the scaling limits and treatment on a case-by-case level: we note that velocity-jump models have received significant attention in the context of cell migration, and we refer to Othmer and Xue (2013) for a review of various classes of movement.

The population distribution generated by the macroscopic model fails to converge with the distributions predicted by the individual-based model for certain parameter regimes. Employing moment closure to derive (5) is just one of various scaling techniques, and we refer to Hillen and Painter (2013) for an overview of other approaches that can be applied to (3). More generally, we note that the continuous mesoscopic velocity-jump model (3) will continue to predict averaged distributions from the individual-based model even when the macroscopic model fails, and can therefore be employed when a continuous approach is required. This approach can also be used *in lieu* of the macroscopic model for cases where the underlying assumptions, such as those described above, are relaxed and the scaling to a macroscopic model is challenging: for example, under the general form of velocity-jump model assumed in (2). Of course, this does come at the cost of reduced tractability: equation (2) is computationally costly, requiring additional discretisation over velocity coordinates, and less amenable to analysis than a macroscopic model such as (5).

A significant, yet highly non-trivial case, emerges when interactions between individuals must be taken into account. For example, the intricate population structures observed in ant trails, bird flocks, fish schools etc. are crucially dependent on communication, whether by direct contact or responses to signalling cues modified by the population, such as pheromones. Formally, deriving a continuous mesoscopic model from the underlying velocity-jump random walk is highly involved: a standard approach is to simply state a model of the form (2) *a priori* (such an example under the current framework is considered in Hillen (2006); Painter (2009) for a cell population interacting by remodelling its local extracellular environment). Rigorously, (2) can only then be viewed as an approximation of the true dynamics, and direct comparisons between its behaviour and the underlying stochastic system should be considered. For example, in Franz et al. (2013) a comparison was made between a stochastic velocity-jump based model and its proposed mesoscopic model for the chemotactic movement of *E. coli* bacteria along consumed nutrient gradients. While the distinct approaches yielded close correspondence over a range of parameter values, notably different behaviour emerged in certain regimes. For simpler interactions a formal derivation of an appropriate continuous model may be possible: for example, see Erban and Haskovec (2012) for an application in locust swarming.

The application to hilltopping explored a number of hypotheses. Firstly, our modelling corroborates the long-standing notion that hilltopping can significantly aid mating (and hence limit population collapses) for low density species (e.g. Shields 1967; Scott 1968): in our virtual population, strong hilltopping neutralised the lower likelihood of meeting a mating partner through co-localisation at summits. Secondly, we demonstrated that the benefit to males of following a hilltopping strategy vary with population density: for low density populations, adopting a hilltopping strategy is highly advantageous, yet at high densities a non-hilltopping strategy proves more successful. These results corroborate the findings suggested in the field studies of Ehrlich and Wheye (1986) and Baughman and Murphy (1988): that hilltopping can be either adaptive or non-adaptive, according to the population density.

The hilltopping model was kept intentionally simple to concentrate on how topography can impose on population dynamics. Butterfly interactions are, of course, considerably more involved than those implied by the model here, and future investigations will aim to address more complicated dynamics. For example, here we restricted to simple forms for emergence, mating and death, equal numbers of males and females and a single density equation that absorbs all of a butterfly's activities (rather than separate equations, with appropriate transitions, for resting, flying, etc.). Furthermore, hilltopping was accounted for via a very simple sensing mechanism: butterflies were postulated to respond to topography by 'computing' the local gradient. Evaluation of the topography is likely to be far more sophisticated in reality: studies in Pe'er et al. (2004) indicate that butterflies determine a direction by assessing the topography within visual range, suggesting that

non-local sampling of the environment is more appropriate. Extending the modelling to evaluate the relative effectiveness of distinct sensing methods will form part of a future study.

An aspect that also demands further attention is the critical role played by vegetation (e.g. see Ehrlich and Hanski 2004; Dover and Settele 2009). First, the distribution of suitable larval vegetation is the determinant for the emergence of new butterflies. Second, its distribution is likely to impact on the orientation of butterflies: for males, perching near sites of emerging females provides an alternative (to hilltopping) mate-locating strategy (Rutowski 1991); for females, proximity to larval food vegetation is advantageous for quickly locating an egg-laying site post-mating. Third, vegetation is of obvious importance in terms of providing a suitable nectar source for feeding. In certain landscapes (for example, the desert landscape in the hilltopping study of Pe'er et al. 2004), exposed hilltops can be devoid of suitable vegetation, creating a dilemma: move to a hilltop or remain near vegetation? Extensions of the model to include heterogeneous vegetation structure will be considered.

We also remark on a number of other simulation studies of hilltopping behaviour. In Pe'er et al. (2005); Peer et al. (2006) an individual-based modelling approach was used to simulate the movement paths of butterflies, based on the hilltopping field study of Pe'er et al. (2004). In particular, topography was shown to channel movement paths along 'virtual corridors'. Findings from the modelling here substantiate these findings: for example, consistent flight paths are observed for butterflies released from the various release sites in Figure 6. In Courtney and Anderson (1986) a game theory approach was used to investigate the distribution of males about encounter sites (such as hilltops). Notably, individuals were assumed to move between locations according to density, and it was shown that no stable distribution was obtained. Our present modelling does not include any behavioural changes due to density-dependence, and this is obviously an important area for further investigation.

The near-ubiquitous importance of spatial structure on the day-to-day activities of mobile organisms is manifested in many crucial questions of conservation biology: How does habitat change impact on the viability of local populations? What are the principal pathways by which an alien species invades? The capacity to generate detailed information on the pathways of animals through GPS and other technologies (e.g. Tomkiewicz et al. 2010) can provide enormous volumes of data to help answer these issues, and its effective use in models is a must if they are to become predictive tools. The modelling here has taken one particular example – butterfly hilltopping – to illustrate a broad multi-scale framework that can be applied to a wide variety of problems: one that passes from an individual-level description of oriented movement paths within a (potentially) spatially-heterogeneous and time-varying environment to a macroscopic-scale model for the evolution of a population.

Appendix: Numerical Methods

Stochastic individual-based model

Each individual starts at $t = 0$ with position and velocity according to the given initial distributions. A movement path is generated through direct simulation of the stochastic velocity-jump process in Matlab. If t_i represents a time at which a turn is made, $\mathbf{x}_i$ is the location of the individual at this time and $\mathbf{v}_{i-1}$ is its previous velocity:

1. The new velocity $\mathbf{v}_i$ is chosen according to the proposed velocity distribution q;

2. The new runtime τ_i is selected from a Poisson distribution, with turning rate parameter λ ($= 1/\tau$, where τ is the mean runtime).
3. The individual is moved to position $\mathbf{x}_{i+1} = \mathbf{x}_i + \tau_i \mathbf{v}_i$, time is incremented to $t_{i+1} = t_i + \tau_i$ and the process is repeated.

For velocity distributions based on the von Mises distribution, we employ code (circ_vmrnd.m) from the circular statistics toolbox (Berens 2009). Selecting an orientation according to this distribution requires a concentration parameter (κ) and dominant angle (ϕ), drawn from the local gradient of an underlying orienteering cue $E(\mathbf{x})$. For landscapes such as Arthur's seat, where terrain data is only available at discrete points, local gradients of E are approximated via a central difference scheme.

Mesoscopic velocity-jump model

Equation (3) is solved using a Method of Lines (MOL) approach: we discretise in position and velocity space to create a large system of ordinary differential equations (ODEs) to be solved with an appropriate time integration method. In two dimensions, with fixed speed s, positional coordinates $(x, y) \in A = [0, L_x] \times [0, L_y]$ are discretised onto a regular lattice $x_1 = \frac{\Delta_x}{2}, x_2 = \frac{3\Delta_x}{2} \ldots, x_M = L_x - \frac{\Delta_x}{2}, y_1 = \frac{\Delta_y}{2}, y_2 = \frac{3\Delta_y}{2} \ldots, y_N = L_y - \frac{\Delta_y}{2}$ for $\Delta_x = L_x/M, \Delta_y = L_y/N$, while velocity $\mathbf{v} = s(\cos\theta, \sin\theta)$ is discretised according to its angular coordinate $\theta \in (-\pi, \pi]$ such that $\theta_1 = -\pi + \Delta_\theta, \theta_2 = -\pi + 2\Delta_\theta, \ldots, \theta_P = \pi$, where $\Delta_\theta = 2\pi/P$,

Spatial terms consist of the advective term representing movement: this is discretised in conservative form via a third-order upwinding scheme, augmented with a flux-limiting scheme to ensure positivity of solutions. The right hand side terms of (3) are treated as kinetic-type terms. Integration of the ODEs has been performed with both explicit and implicit schemes: the former a forward Euler method with sufficiently small time step, the latter with the ROWMAP stiff systems integrator (Weiner et al. 1997). Tests using the two time-iteration methods yield equivalent results and simulations have been performed across a range of discretisation steps. Default discretisations for the simulations employ $N = M = 200$ and $P = 100$.

Macroscopic model

We also employ a MOL scheme to solve the macroscopic equation (5). The spatial region A is discretised using the same regular lattice as above for the transport model. In 2D, assuming the drift-vector and diffusion-tensor are of the form

$$\mathbf{a}(x, y) = \begin{pmatrix} \mu(x, y) \\ \nu(x, y) \end{pmatrix} \text{ and } \bar{D}(x, y) = \begin{pmatrix} \alpha(x, y) & \gamma(x, y) \\ \gamma(x, y) & \beta(x, y) \end{pmatrix},$$

we can expand the spatial terms of (5) as follows

$$-\nabla(\mathbf{a}u) + \nabla\nabla(\bar{D}u) = (\alpha u_x)_x + (\gamma u_x)_y + (\gamma u_y)_x + (\beta u_y)_y$$
$$+ ((\mu + \alpha_x + \beta_y)u)_x + ((\nu + \beta_x + \gamma_y)u)_y.$$

The above reveals a combination of diffusive (first line) and advective (second line) type-terms, with the diffusive terms in the first line identical to those generated for standard anisotropic diffusion.

The choice of finite-difference discretisation for diffusive terms is crucial: naive discretisations can lead to numerical instability for large and negative γ, see Mosayebi et al. (2010). The possibility of numerical instability can be reduced using the method in Weickert (1998): finite difference derivatives are calculated not only along the 'standard' axes of the lattice, but combined with those in an appropriately chosen new direction. Advective terms are discretised in conservative form,

employing a first-order upwinding scheme. Time integration involves a forward Euler method with a suitably small time-step Δt. To verify the numerical method, simulations have been performed for varying time-step and mesh-discretisations. The validity of the various numerical methods is further substantiated by convergence of the models within relevant regimes.

References

J. Alcock. Leks and hilltopping in insects. *J. Nat. Hist.*, 21:319–328, 1987.

J.F. Baughman and D.D. Murphy. What constitutes a hill to a hilltopping butterfly? *Amer. Mid. Nat.*, 120:441–443, 1988.

J.F. Baughman, D.D. Murphy, and P.R. Ehrlich. Population structure of a hilltopping butterfly. *Oecologia*, 75: 593–600, 1988.

P. Berens. Circstat: A matlab toolbox for circular statistics. *J. Stat. Soft.*, 31:1–21, 2009.

M.D. Bowers, I.L. Brown, and D. Wheye. Bird predation as a selective agent in a butterfly population. *Evolution*, 39:93–103, 1985.

E.T. Cant, A.D. Smith, D.R. Reynolds, J.L. Osborne, E.T. Cant, A.D. Smith, D.R. Reynolds, and J.L. Osborne. Tracking butterfly flight paths across the landscape with harmonic radar. *Proc. Roy. Soc. B: Biol. Sci.*, 272: 785–790, 2005.

R. S. Cantrell and C. Cosner. *Spatial ecology via reaction-diffusion equations*. Wiley, 2004.

E. A. Codling, M. J. Plank, and S. Benhamou. Random walk models in biology. *J. Roy. Soc. Interface*, 5:813–834, 2008.

E. A. Codling, R. N. Bearon, and G. J. Thorn. Diffusion about the mean drift location in a biased random walk. *Ecology*, 91:3106–3113, 2010.

S. P. Courtney and K. Anderson. Behaviour around encounter sites. *Behav. Ecol. and Sociobiol.*, 19:241–248, 1986.

J. Dover and J. Settele. The influences of landscape structure on butterfly distribution and movement: a review. *J. Insect Cons.*, 13:3–27, 2009.

P. R. Ehrlich and I. Hanski. *On the wings of checkerspots: a model system for population biology*. Oxford University Press, USA, 2004.

P. R. Ehrlich, A. E. Launer, and D. D. Murphy. Can sex ratio be defined or determined? The case of a population of checkerspot butterflies. *Amer. Nat.*, 124:527–539, 1984.

P.R. Ehrlich and D. Wheye. "Nonadaptive" hilltopping behavior in male checkerspot butterflies (euphydryas editha). *Amer. Nat.*, 127:477–483, 1986.

R. Erban and J. Haskovec. From individual to collective behaviour of coupled velocity jump processes: A locust example. *Kin. Rel. Mod.*, 5:817–842, 2012.

B. Franz, C. Xue, K.J. Painter, and R. Erban. Travelling waves in hybrid chemotaxis models. *Submitted*, 2013.

I. Hanski. *Metapopulation ecology*. Oxford University Press, Oxford, UK, 1999.

J. J. Hellmann, S. B. Weiss, J. F. Mclaughlin, C. L. Boggs, P. R. Ehrlich, A. E. Launer, and D. D. Murphy. Do hypotheses from short-term studies hold in the long-term? An empirical test. *Ecol. Entomol.*, 28:74–84, 2003.

T. Hillen. Transport equations with resting phases. *Eur. J. Appl. Math.*, 14:613–636, 2003.

T. Hillen. M5 mesoscopic and macroscopic models for mesenchymal motion. *J. Math. Biol.*, 53:585–616, 2006.

T. Hillen and K. J. Painter. *Dispersal, individual movement and spatial ecology: a mathematical perspective*, chapter Transport and anisotropic diffusion models for movement in oriented habitats, pages 177–222. Springer, Berlin, Heidelberg, 2013.

T. Hillen, K. J. Painter, and M. Winkler. Anisotropic diffusion in oriented environments can lead to singularity formation. *Eur. J. Appl. Math.*, 24:371–413, 2013.

Y. Iwasa, F. J. Odendaal, D. D. Murphy, P. R. Ehrlich, and A. E. Launer. Emergence patterns in male butterflies: a hypothesis and a test. *Theor. Pop. Biol.*, 23:363–379, 1983.

F. M. Jiggins, G. D. D. Hurst, and M. E. N. Majerus. Sex-ratio-distorting wolbachia causes sex-role reversal in its butterfly host. *Proc. Roy. Soc. Lond. B: Biol. Sci.*, 267:69–73, 2000.

P. M. Kareiva and N. Shigesada. Analyzing insect movement as a correlated random walk. *Oecologia*, 56:234–238, 1983.

J. G. Kingsolver. Thermoregulation and flight in colias butterflies: elevational patterns and mechanistic limitations. *Ecology*, 64:534–545, 1983.

K. V. Mardia and P. E. Jupp. *Directional Statistics*. Wiley, New York, 2000.

H. W. McKenzie, E. H. Merrill, R. J. Spiteri, and M. A. Lewis. How linear features alter predator movement and the functional response. *Roy. Soc. Interface Focus*, 2:205–216, 2012.

P. Moorcroft and M. A. Lewis. *Mechanistic home range analysis*. Princeton University Press, USA, 2006.

P. Mosayebi, D. Cobzas, M. Jagersand, and A. Murtha. Stability effects of finite difference methods on a mathematical tumor growth model. In *Computer Vision and Pattern Recognition Workshops (CVPRW), 2010 IEEE Computer Society Conference on*, pages 125–132. IEEE, 2010.

A. Okubo and S. A. Levin. *Diffusion and ecological problems: modern perspectives*. Springer Verlag, 2001.

H. G. Othmer and C. Xue. *Dispersal, individual movement and spatial ecology: a mathematical perspective*, chapter The Mathematical Analysis of Biological Aggregation and Dispersal. Springer, Berlin, Heidelberg, 2013.

H. G. Othmer, S. R. Dunbar, and W. Alt. Models of dispersal in biological systems. *J. Math. Biol.*, 26:263–298, 1988.

K. J. Painter. Modelling cell migration strategies in the extracellular matrix. *J. Math. Biol.*, 58:511–543, 2009.

K. J. Painter and T. Hillen. Mathematical modelling of glioma growth: The use of diffusion tensor imaging (DTI) data to predict the anisotropic pathways of cancer invasion. *J. Theor. Biol.*, 323:25–39, 2013.

C. S. Patlak. Random walk with persistence and external bias. *Bull. Math. Biol.*, 15:311–338, 1953.

G. Pe'er. *Spatial and Behavioral Determinants of Butterfly Movement Patterns in Topographically Complex Landscapes*. PhD thesis, PhD thesis, Ben-Gurion University of the Negev, 2003.

G. Pe'er, D. Saltz, H. H. Thulke, and U. Motro. Response to topography in a hilltopping butterfly and implications for modelling nonrandom dispersal. *Anim. Behav.*, 68:825–839, 2004.

G. Pe'Er, D. Saltz, and K. Frank. Virtual corridors for conservation management. *Conservation biology*, 19:1997–2003, 2005.

G. Peer, S.K. Heinz, and K. Frank. Connectivity in heterogeneous landscapes: analyzing the effect of topography. *Land. Ecol.*, 21:47–61, 2006.

J. Roland, N. Keyghobadi, and S. Fownes. Alpine parnassius butterfly dispersal: effects of landscape and population size. *Ecology*, 81:1642–1653, 2000.

R. L. Rutowski. The evolution of male mate-locating behavior in butterflies. *Amer. Nat.*, 138:1121–1139, 1991.

J.A. Scott. Hilltopping as a mating mechanism to aid the survival of low density species. *J. Res. Lepid*, 7:191–204, 1968.

J.A. Scott. Lifespan of butterflies. *J. Res. Lepid.*, 12:225–230, 1973a.

J.A. Scott. Mating of butterflies. *J. Res. Lepid.*, 11:99–127, 1973b.

O. Shields. Hilltopping. *J. Res. Lepid*, 6:69–178, 1967.

JG Skellam. Random dispersal in theoretical populations. *Biometrika*, 38:196–218, 1951.

S. M. Tomkiewicz, M. R. Fuller, J. G. Kie, and K. K. Bates. Global positioning system and associated technologies in animal behaviour and ecological research. *Phil. Trans. Roy. Soc. B: Biol. Sci.*, 365:2163–2176, 2010.

P. Turchin. *Quantitative analysis of movement: measuring and modeling population redistribution in animals and plants*. Sinauer Associates, Sunderland, 1998.

P. Turchin, FJ Odendaal, and MD Rausher. Quantifying insect movement in the field. *Environ. Entomol.*, 20:955–963, 1991.

J. Weickert. *Anisotropic diffusion in image processing*. Teubner, Stuttgart, 1998.

R. Weiner, B.A. Schmitt, and H. Podhaisky. Rowmapa row-code with krylov techniques for large stiff odes. *Applied numerical mathematics*, 25:303–319, 1997.

P. O. Wickman. Dynamics of mate-searching behaviour in a hilltopping butterfly, lasiommata megera (l.): the effects of weather and male density. *Zool. J. Linn. Soc.*, 93:357–377, 1988.